2016-12-27

Bromine soil/sediment enrichment in tidal salt marshes as a potential indicator of climate changes driven by solar activity: New insights from W coast Portuguese estuaries

Moreno, J

10.1016/j.scitotenv.2016.11.130
Science of The Total Environment
Elsevier BV

Bromine soil/sediment enrichment in tidal salt marshes as a potential indicator of climate changes driven by solar activity: new insights from W coast Portuguese estuaries

J. Moreno[a,b,1], F. Fatela[a,b], E. Leorri[c], F. Moreno[d], M.C. Freitas[a,b], T. Valente[e], M.F. Araújo[f], J.J. Gómez-Navarro[g], L. Guise[e] and W.H. Blake[h]

[a] IDL - Instituto Dom Luiz, Universidade de Lisboa, Campo Grande, 1749-016 Lisboa, Portugal.

[b] Departamento de Geologia da Faculdade de Ciências da Universidade de Lisboa, Campo Grande, 1749-016 Lisboa, Portugal.

[c] East Carolina University, Department of Geological Sciences, Greenville, NC 27858-4353, USA.

[d] Independent researcher, Caminho da Portela, 97, 4940-061 Bico PCR, Portugal.

[e] Universidade do Minho, Centro de Investigação Geológica, Ordenamento e Valorização de Recursos, Departamento de Ciências da Terra, CIG-R, 4710-057 Braga, Portugal.

[f] Universidade de Lisboa, Instituto Superior Técnico, Centro de Ciências e Tecnologias Nucleares (C^2TN), Estrada Nacional 10, km 139,7, 2695-066 Bobadela LRS, Portugal.

[g] Department of Physics, University of Murcia, Spain.

[h] School of Geography, Earth and Environmental Sciences, Plymouth University, Plymouth, Devon, PL4 8AA, UK

[1] jcmoreno@fc.ul.pt

Abstract

This paper aims at providing insight about bromine (Br) cycle in four Portuguese estuaries: Minho, Lima (in the NW coast) and Sado, Mira (in the SW coast). The focus is on their tidal marsh environments, quite distinct with regard to key biophysicochemical attributes. Regardless of the primary bromide (Br^-) common natural source, i.e. seawater, the NW marshes present relatively higher surface soil/sediment Br concentrations than the ones from SW coast. This happens in close relation with organic matter (OM) content, and is controlled by their main climatic context. Yet, the anthropogenic impact on Br concentrations cannot be discarded. Regarding [Br] spatial patterns across the marshes, the results show a general increase from tidal flat towards high marsh. Maxima [Br] occur in the upper driftline zone, at transition from highest low marsh to high marsh, recognized as a privileged setting for OM accumulation. Based on the discovery of OM ubiquitous bromination in marine and transitional environments, it is assumed that this Br occurs mainly as organobromine. Analysis of two dated sediment cores indicates that, despite having the same age (AD 1300), the Caminha salt marsh (Minho estuary) evidences higher Br enrichment than the Casa Branca salt marsh (Mira estuary). This is related to a greater Br storage ability, which is linked to OM build-up and rate dynamics under different climate scenarios. Both cores evidence a fairly similar temporal Br enrichment pattern, and may be interpreted in light of the sun–climate coupling. Thereby, most of the well-known Grand Solar Minima during the Little Ice Age appear to have left an imprint on these marshes, supported by higher [Br] in soils/sediments. Besides climate changes driven by solar activity and impacting marsh Br biogeodynamics, those [Br] positive peaks might also reflect inputs of enhanced volcanic activity covarying with Grand Solar Minima.

Keywords: Salt marshes; Br cycle; OM storage; Grand Solar Minima; Climate modelling; Climate variability.

1. Introduction

Wetlands play an important role on the biogeochemical cycle of elements such as carbon, nitrogen, phosphorus, sulphur and mercury at local, regional and even global scales (e.g., Marques et al., 2011; Neubauer et al., 2013). A considerable amount of research has revealed that this is also true for bromine (Br) (Varner et al., 1999; Keppler et al., 2000; Rhew et al., 2000, 2002, 2014; Dimmer et al., 2000; Drewer et al., 2006; Manley et al., 2006; Hardacre et al., 2009, 2013; Blei et al., 2010; Martínez-Cortizas et al., 2007, 2016). Specifically, coastal wetlands, in which tidal marshes are included, represent important land-ocean-atmosphere interfaces that allow to capture spatiotemporal variability in chemical fluxes. In these habitats, Br mainly supplied by seawater interacts with both halophytes and the relatively large pool of soil/sediment organic matter (OM). This connection occurs through, although still poorly understood, bromination processes that contribute to the production of organobromine compounds, which have detrimental effects on the atmosphere. For instance, salt marshes have been identified as globally significant natural sources of methyl bromide (CH_3Br) (Rhew et al., 2014, and references therein), a reactive trace gas contributing to ozone loss processes in the stratosphere (e.g., Chipperfield, 2015). On the other hand, significant widespread bromination of natural OM may significantly impact the preservation and/or degradation of organic carbon (C_{org}) in soils/sediments (Leri and Myneni, 2012), therefore affecting the recognized salt marsh ecosystem's role on climate and carbon sequestration. It is also known that in coastal (and open ocean) areas, bromine-radical chemistry provides alternative reaction pathways in the marine atmospheric boundary layer for (i) sulphur cycling, with associated implications for

aerosol production (and growth), radiative heat transfer and climate (Keene et al., 2007), and (ii) mercury (Hg) cycling (Obrist et al., 2011; Tas et al., 2012), with Br-induced mercury oxidation as a likely important Hg source to world's oceans, which can contribute to human mercury exposure by seafood consumption (Sunderland, 2007). Taking together the previous findings about the Br influence on other key element biogeochemical cycles in the marine domain, and the knowledge that natural CH_3Br emissions are contributing to increase the stratospheric reactive Br budget (e.g., Carpenter et al., 2014), establishing the foundations of the Br biogeochemical cycle in coastal areas and tidal marsh habitats has gained a renewed significance.

Traditionally, Br has been used in conjunction with chlorine (Cl) as a geochemical proxy for seawater intrusion in coastal areas (e.g., Jones et al., 1999; Alcalá and Custodio, 2008), and alone as a paleosalinity indicator and a stratigraphic marker in brine cores (Adams, 1969; Ziegler et al., 2008). An alternative interpretation regarding Br concentrations and fluxes has been proposed by Moreno et al. (2015) when studying the sedimentary record recovered from the high marsh zone on a tidal salt marsh located in the NW coast of Portugal (Caminha, in the Minho River estuary). They suggested that the most prominent Br enrichment peaks between AD 1300 (tidal marsh settlement) and AD 1800 (considered as the beginning of industrialization) were primarily driven by a series of biogeochemical processes rather than an indication of seawater intrusion events in the Minho estuary. Those processes responded to significantly prolonged environmental (e.g., temperature and precipitation) shifts triggered by Grand Minima Episodes of solar activity (SA) during the LIA, namely the Wolf and the Maunder Minima, as well as the Dalton Minimum. These episodes corresponded to periods of solar minimal energy output, as demonstrated by long-term records of SA proxies (e.g. Usoskin et al., 2007), affecting Earth's climate. Prolonged changes in environmental conditions can lead to significant responses at all levels of ecosystem organization, generating persistent alterations in its biogeochemical functioning

(e.g., Keller et al., 2006; Neubauer et al., 2013). Accordingly, and based on Moreno et al. (2015) that linked Br biogeodynamics to past SA, the impact of the sun–climate coupling at Grand Solar Minima resulted in cascading effects on Br cycling in the Caminha salt marsh, in parallel with rate changes in OM bromination, which ultimately weakened the marsh's role as a source for CH_3Br.

Following the study conducted in Caminha, the current contribution expands and generalises the analysis, including three other Portuguese estuaries (Figure 1): the Lima estuary, also in the NW coast, and the Sado and Mira estuaries, both located in the SW coast. Broadly, the Portuguese W coast is typically characterized by an Atlantic climate, though two main climatic regions can be distinguished. Compared to the NW coast, climate in SW coast has drier summers, lower annual precipitation as well as higher annual temperatures and insolation. Therefore, the aim of this work is twofold: (i) acquire a wider latitudinal range of Br measurements in waters (superficial and interstitial) and marsh soils/sediments in order to infer trends associated to the bio-geomorphological settings and climatic variability, and (ii) improve the understanding of bromine-climate relationships driven by SA, also providing new independent data and source insight to the still ongoing debate about the "missing source" for the CH_3Br global budget (Yvon-Lewis et al., 2009).

2. Regional setting

NW coast

Taken together, the Minho and Lima watersheds cover an area of 19 550 km^2 under an Atlantic wet climate, with relatively high exposition to maritime winds, high mean annual precipitations (Minho: 1200–2400 mm; Lima: 1300–4200 mm), mild summers (summer

mean temperatures from ca. 18–22ºC) and relatively low mean annual insolation (2200–2500 hours) (APA, 2011).

The Minho estuary (23 km^2) is oriented NE–SW and presents a semidiurnal, high-mesotidal regime in which vertical stratification occurs during periods of large freshwater discharge. The mean annual freshwater inflow is around 300 m^3/s (Ferreira et al., 2003). The highest high water spring (HHWS) is 4 m height, but this is often amplified by storm surges (Taborda and Dias, 1991), which we observed during field work. The mean tidal range is of about 2.0 m. The upstream limit of the tidal salt wedge in the Minho River is 9 km (Fatela et al., 2009). Large tidal flat and tidal marsh surfaces with approximately 6 km^2 occur in the Minho estuary's banks, with its largest expansion along the left bank – Caminha tidal marsh (ca. 2.5 km^2) – at the confluence with Coura tributary (Figure 1). Recently, Reis et al. (2014) updated the estuary ecological quality to "moderately to remarkably polluted" based on metal concentrations guidelines (SFT TA-1467/1997). Furthermore, the use of ethylene dibromide in leaded gasoline and the vehicle emissions since 1930, a shared Br and Pb anthropogenic source, appears to have had a significant impact on the Caminha salt marsh (Moreno et al., 2015).

The Lima estuary (5 km^2), located 20 km south of Minho, is oriented ENE–WSW and it is a semidiurnal mesotidal estuary, with a mean tidal range of about 2.5 m and a HHWS of 3.7 m (Vale and Dias, 2011). The mean annual freshwater inflow is 50 m^3/s (Vale and Dias, 2011). Here the tidal salt wedge effect is noticed to 3–5 km upstream in winter and no more than 15 km in summer (Alves, 2003). Intertidal areas extend over more than 2 km^2 on the banks of the Lima estuary, including the Nossa Senhora do Rosário salt marsh (NSR; Figure 1). The Lima lower estuary's ecological status is considered moderate (Costa-Dias et al., 2010). This results from the significant impact on the estuary of the harbour activities, leading to continuous petrochemical contamination (Lima et al., 2007), and diffuse pollution

146 from agriculture, domestic, and industrial waste discharges, including a paper mill (Costa-
147 Dias et al., 2010).

148 The salt marshes of these two NW sites are classified as Eurosiberian, based on their plant
149 communities (Costa et al., 2009), with abundant reed meadows where the presence of
150 *Juncus maritimus* Lam. (C3 plant; non-succulent; perennial) is ubiquitous (Honrado et al.,
151 2004; Almeida et al., 2011). Although, other plant species can also be found such as the
152 non-native *Triglochin striatum* Ruiz & Pav. (C3 plant; succulent; perennial), the invasive
153 *Phragmites australis* (Cav.) Trin ex. Steud. (C3 plant) and the weed *Spartina patens* (Aiton)
154 Muhl (C4 plant; non-succulent; perennial) (Almeida et al., 2011).

155

156 ***SW coast***

157 The SW coast of Portugal, where the Sado and Mira estuaries are located, is under a sub-
158 wet Mediterranean climate, with mean values of annual precipitation around 600–700 mm
159 (Bettencourt et al., 2003). Mean air surface temperatures are near 23ºC in the hottest
160 months (July and August), with a yearly average number of sunshine hours ranging 2900–
161 3000 (APA, 2011), also showing almost permanent maritime moist winds (APA, 2011). The
162 size of Sado and Mira rivers watersheds is 6 700 km^2 and 1 576 km^2, respectively.

163 The Sado estuary (170 km^2), the second largest estuarine system in Portugal, is located
164 about 40 km south of Lisbon (Figure 1). It is a well-mixed estuary under normal river flow
165 conditions, however, high discharge in some winter months may cause moderate
166 stratification locally (Ferreira et al., 2003). It has a complex morphology generally oriented
167 NW–SE and presents wide tidal flats as well as narrow and discontinuous coastal salt
168 marshes covering around 7.2 km^2 (Moreira, 1992). The tidal pattern is semi-diurnal, with a
169 mean tidal range of about 2.7 m and a HHWS of 3.2 m (Martins et al., 2001). The maximum

salt-wedge limit is 70 km upstream. The mean annual freshwater input is ca. 40 m^3/s, exhibiting large interannual fluctuations. The lower estuary behaves as a coastal lagoon, while the upper reaches present a greater fluvial influence (Martins et al., 2001). In general, the Sado estuary can be classified as moderately contaminated, but the lower estuary and some segments near industrial areas have revealed levels of concern for several contaminants both organic and inorganic, with adverse toxicological effects to biota (e.g., Neuparth et al., 2005).

Finally, the vertically well-mixed Mira estuary (4.5 km^2) is a narrow incised estuary oriented NE–SW (e.g., Paula et al., 2006). It presents a semi-diurnal mesotidal regime with a mean tidal range of about 2.4 m and a HHWS of 3.5 m (Amaral et al., 2007). The salt edge may reach 32 km from the river mouth (Bettencourt et al., 2003). The lower section of the estuary has a dominant marine influence due to low, seasonal and limited freshwater input by the Mira River (2.9 m^3/s). This characteristic has allowed the development in the lower 8 km of large, intertidal, and homogenous seagrass meadows of *Zostera noltii* Hornemann, 1832 (e.g., Cunha et al., 2013). The estuarine area is also characterized by bare sandy areas and muddy substrates, with a 2.9 km^2 area of fringing salt marshes occurring as far as 15–20 km upstream (Costa et al., 2001). These salt marshes have remained nearly unchanged since 1958, with the entire ecosystem relatively undisturbed by anthropogenic activities (Castro and Freitas, 2006).

As oppose to the NW sites, the SW salt marshes studied here belong to the Biogeographic Mediterranean region (Costa et al., 2009). The halophytic community is mixed including perennial succulent species such as *Halimione portulacoides* (L.) Aellen (C3 plant), *Sarcocornia fruticosa* (L.) A.J. Scott (C3 plant), *Sarcocornia perennis* (Mill.) A.J. Scott (C3 plant) in the high marsh and the annuals *Spartina maritima* (Curtis) Fernald (C4 plant) and *Salicornia fragilis* P. W. Ball & Tutin (C3 plant) in the low marsh (e.g., Costa, 2001).

2. Materials and Methods

2.1. Water and sediment samples

The methodologies used for sampling and analysis of water (superficial and interstitial) and sediments (surface and cored) in the Lima, Sado and Mira estuaries follow Moreno et al. (2015) and are fully described therein. Figure 1 and Tables 1 and 2 summarize the new samples analysed here: eight interstitial water samples from three salt marsh transects (NSR_L, TRO_S, PMF_M), ninety-one sediment surface samples from the intertidal domain (tidal flat, devoid of vascular plants; low marsh and high marsh zones with typical halophytic vegetation), along ten cross-shore transects, as well as an one-metre-long sediment core (hereafter FWCBr) recovered with a manual Auger sampler from the Casa Branca salt marsh (1.74 m above mean sea level; 37°40′03.7″ N and 8°43′12.7″ W), located on the Mira River estuary. A total of thirty sliced (1 cm thick) samples were analysed for Br and OM contents. The FCPw1 core from Moreno et al. (2015), located in the Caminha high marsh zone (1.55 m above mean sea level; 41°52′37.0″ N and 8°49′28.0″ W), is also indicated in Figure 1.

In order to characterize the two possible end-members (fluvial and marine) of biogeochemical sources to salt marshes, four marine seawater and four fluvial freshwater samples were collected (Table 1).

Water sample analyses: The filtrate was analysed for bromide (Br^-), amongst other anions, by ion chromatography (IC) with suppressed conductivity detection (761 Compact IC Metrohm), and raw data processed with Metrohm Metro data 1.1. The IC method no. S-73, developed by Metrohm to determine anions in seawater, was used for the most saline waters (see Valente et al., 2009 and Moreno et al., 2015 for detailed information). A set of

219 standards was prepared to make a 6-point calibration curve covering the range of Br^- (and
220 Cl^-) concentrations in water samples. The IC method not only allows an efficient separation
221 of the Br^- and Cl^- peaks, but has also the advantage of measuring both anions in the same
222 sample preventing the errors introduced by dilution. A standard (20 mg/L) was run
223 independently of the calibration curve to check for accuracy (every two samples) and
224 sample replicates were run to check for precision. The precision was within the relative
225 standard deviation (RSD) of 5% for all determinations and results were accurate within
226 precision.

227 Sediment sample analysis: Br concentrations in cored samples, along with the collected
228 surface sediments, were determined by Energy-Dispersive X-Ray Fluorescence
229 Spectrometry (EDXRF), using a KEVEX 771 spectrometer. To calibrate the spectrometer
230 and verify the accuracy and precision of the overall procedure three certified reference
231 materials were analysed: SGR1 (Green River Shale from the United States Geological
232 Survey – USGS), SRM 2704 (Buffalo River Sediment) and SRM1646 (Estuarine Sediment),
233 both from the National Institute for Standards and Technology (NIST). A complete
234 description of the equipment, analytical conditions and spectral evaluation, along with the
235 calibration and quantification techniques, is available in Araújo et al. (1998, 2003). Accuracy
236 and precision on the Br determinations are better than 10% as previously fully described in
237 Moreno et al. (2015). The OM content was determined as Loss-on-Ignition (LOI), with an
238 aliquot of bulk sediment sample (2.0 g) dried and oven-heated at a temperature of 500 ºC ±
239 50 ºC for about 2 hours (Moreira et al., 2009). Quality control was checked by replicate
240 analysis (40% of the total), with errors lying in the interval 0.1%–15.0% (average: 5.7%) of
241 the measured value. In an attempt to test the reliability of LOI data for the estimation of C_{org}
242 content, a regression analysis was performed for LOI *vs.* C_{org} for the FCPw1 core, with C_{org}
243 data taken from de la Rosa et al. (2012). A strong statistically significant correlation (r= 0.97,

N= 19; $p < 0.001$) between LOI and C_{org} was achieved, ensuring that LOI results are reflecting mostly C_{org} (%OM).

In order to characterize OM quality, i.e. the percentages of labile and recalcitrant OM, the stepwise thermogravimetric procedure (STG) of Kristensen (1990) was applied to the cored samples from the Casa Branca salt marsh. According to this method, these OM fractions are defined as the percentage weight losses after ignition at 280ºC and 520ºC, respectively. In short, samples of 0.5 g were grounded and pre-dried at 105ºC for 6h. After cooling in a desiccator, the sample weight was determined with a precision of 0.1 mg. Next, the samples were combusted at precisely 280ºC for 6h in a computer controlled Heraeus MR 170 muffle furnace. After cooling in a desiccator and re-weighting, the samples returned to the muffle furnace and combusted at 520ºC for 6h. After cooling in a desiccator the final ash weight was determined (Kristensen, 1990).

2.2. Solar activity, temperature, and precipitation climatic modelled data

Cosmogenic radionuclides are produced in the atmosphere through a nuclear cascade mainly triggered by the high-energy galactic cosmic rays (GCR; Lal and Peters, 1967). As GCR enter the heliosphere, they are subject to modulation processes due to variable solar magnetic activity. This is the reason why during phases of low SA much higher particle intensities occur inside the heliosphere than during solar maximum conditions (e.g., Herbst et al., 2015; Adolphi and Muscheler, 2016). The two most noticeable cosmogenic radionuclides suitable for reconstructing SA are ^{14}C and ^{10}Be. The production rate of both isotopes reacts in a very similar way to changes in solar and geomagnetic shielding (Masarik and Beer, 1999). The reconstructed dataset chosen for this work is the total solar irradiance (TSI), considered as a proxy for SA, from Steinhilber et al. (2012). This

reconstruction is based on time series of ^{14}C stored in tree rings and of ^{10}Be extracted from polar ice cores, and was downloaded from the NOAA web page (http://www.noaa.gov/).

Aiming to compare the Br and OM records with climate variables, this study also incorporates the series of temperature and precipitation evolution in both study areas as predicted by a high-resolution regional climate model (Gómez-Navarro et al., 2011). The simulation implements a domain that encompasses the whole Iberian Peninsula (IP) and spans the second millennium entirely. It was carried out with a climate version of the mesoscale model MM5, and driven at the boundaries by a simulation with the global model ECHO-G (see Gómez-Navarro et al., 2011 for details). Following Gómez-Navarro et al. (2011), the use of a high resolution model aims to reduce the scale gap between the large-scale correctly simulated by the GCM and the features of regional variability present in the Br and OM records presented here. The model simulates coherently the evolution of most relevant climate variables, and in particular reproduces the physically constrained co-evolution of temperature and precipitation, as well as their relation with large-scale dynamics (e.g., the North Atlantic Oscillation – NAO). It is jointly driven by reconstructions of the variability of three external forcings: TSI, greenhouse gas concentrations and the effect of volcanic activity.

2.3. Chronology

The geochronology of the top 15 cm of the FWCBr core was calculated from the ^{210}Pb profile using the constant rate of supply method (CRS) (Appleby and Oldfield, 1978) supported by ^{137}Cs. Samples for ^{210}Pb and ^{137}Cs were analyzed following the methodology described by Appleby (2001) at the University of Plymouth (UK) Consolidated Radioisotope Facility, using an EG&G Ortec planar (GEM-FX8530-S N-type) HPGe gamma spectrometry

system built to ultra-low background specification for 210Pb detection. Additional information regarding the technique is provided in Appendix A. This core presented an unsupported ^{210}Pb (^{210}Pbxs) profile that suggested some changes in the sediment accumulation rate in the upper section (*ca.* 150 years), although they could also reflect sediment mixing or disruption of the sedimentation. While the available elemental data is limited and presents generally low concentrations, the Pb profile shows slightly higher values above 18 cm that could be coincident with the initial stages of the industrial revolution (unclear date for this region but *ca.* AD 1800), which would be in agreement with the CRS model used here. However, the inflexion indicated by the model for the two older samples should be considered carefully (Leorri et al., 2010). In order to extend the chronology down-core, two samples (69–70 cm, 90–91 cm depth) of total organic carbon (TOC) were carbon-14 dated by accelerator mass spectrometry–AMS at Beta Analytic Inc. (USA). The chronology for the FWCBr core was created using a Bayesian age-depth model (Bchron 4.1; Haslett and Parnell, 2008; Parnell et al., 2008) (Appendix A). The model provides ages with an individual error for each sample averaging 73 years for a 95% confidence interval. The obtained calendar ages are presented in years of *Anno Domini* (years AD).

The chronology of the FCPw1 core can be found in Moreno et al. (2015), but also relies on the combination of ^{210}Pb and carbon-14 data from TOC.

3. Results and discussion

3.1. Br^- in surface and interstitial water samples

The results of Br^- concentrations in surface and interstitial waters are presented in Table 1. Freshwater samples show Br^- contents between less than 0.01 mg/L (Minho River) and a

316 maximum of 0.8 mg/L (Sado River). On the other hand, marine surface water samples
317 throughout the W coast have Br^- contents ranging from 185 to 197 mg/L (Table 1). Such
318 high values, outside the typical marine [Br^-] range: 60–80 mg/L, are somewhat expected
319 and connected or linked to the known supersaturation in brominated organic compounds in
320 the Portuguese offshore (Raimund et al., 2011). This is related to the presence of strong
321 macroalgal sources and to the Iberian Peninsula coastal upwelling, as discussed previously
322 by Moreno et al. (2015). Brominated organic compounds (also including CH_3Br) are
323 produced and degraded at relatively fast rates in the coastal ocean, with their degradation
324 mechanisms (e.g., hydrolysis and chloride exchange reactions) in the water column as
325 major suppliers of bromide anions to seawater. Our hypothesis – linking the Br^- enrichment
326 of western Portuguese superficial coastal waters to loss reactions of brominated organic
327 compounds in seawater column – may be supported by other authors' findings. Namely, Hu
328 et al. (2010) discovered for the east coast of United States evidence of a vertical distribution
329 in the CH_3Br saturation anomalies, with highest concentrations in the subsurface seawater
330 below the mixed layer, due to high degradation rates near the surface. An analogous
331 subsurface seawater enhancement in depth profiles of two of the most important short-lived
332 carriers of atmospheric Br, i.e. dibromomethane (CH_2Br_2) and bromoform ($CHBr_3$), was
333 described by Raimund et al. (2011) when sampling the Iberian Peninsula upwelling system
334 off the coast of Portugal.

335 The detected Br^- enrichment in the nearshore surface water samples also implies that
336 marine water would have Cl^-/Br^- mass ratios lower than the reported value for the average
337 seawater (typically 290 ± 4; e.g., Katz et al., 2011). This chemical signature in our water
338 samples is presented in the plot of Cl^-/Br^- mass ratios versus Cl^- in Figure 2, along with a
339 typical marine water sample (TA_SW: [Cl^-] = 19,353 mg/L and [Br^-] = 67 mg/L; Millero,
340 2013). The clusters displayed by the Cl^-/Br^- *vs.* Cl^- plot allow to identify freshwater (with
341 consistently lower levels of Cl^- and Br^-) from marine and brackish waters reflecting an

increase in Cl^- (Figure 2A). In addition, it is possible to differentiate between the interstitial water samples of the NW coast salt marshes (Minho and Lima) and the SW coast samples (Sado and Mira) (Figure 2B). This suggests that beyond the inferred common main source of Br^- (and Cl^-), i.e., seawater (theoretical ranges after Panno et al., 2006), a clear N–S differentiation can be established based on the relationship between the chemical indicators chloride and bromide. As shown in Figure 2B, the Sado and Mira interstitial waters, ranging from polyhaline (18–30‰) to euhaline (30–40‰), can be considered closer, based on these anions, to marine water samples (all clustering together; Figure 2B) than the ones from the Caminha and Lima salt marshes (mostly mesohaline: 5–18‰). These results are symptomatic of a stronger mixing with freshwater, originated by higher inputs of rainfall-land runoff production to the NW coast salt marshes, leading to salt dilution and lower ionic concentrations.

At this point, it must be emphasized that a rising body of evidence suggests that Br^- does not act conservatively in soils or water. Br^- can be (re)actively involved in OM cycling (e.g., Gerritse and George, 1988; Mahn and Gieskes, 2001; Biester et al., 2004, 2006; Leri et al., 2010, 2014), and it is frequently related to Fe and Mn cycling (e.g., Leri et al. 2010). This could diminish the "sensitivity" of the ratio Cl^-/Br^-, and limits its applicability as an inorganic tracer of marine intrusion. However, plotting Cl^-/Br^- ratios provides insight into the Br^- (and Cl^-) major sources in the sampled salt marshes. Panno et al. (2006) proposed Cl^-/Br^- fingerprinting as a valuable diagnostic method in the identification of anthropogenic sources of salinization; though additional analysis should be required to complement this technique, and thus determine more accurately the source of the contaminant present in water samples. For instance, Figure 2B depicts a group of samples that evidence an anthropogenic impact based on this methodology – NSR_P1 (tidal flat; Lima), TRO_P7 (high marsh zone; Sado) and PMF_P6 (high marsh zone; Mira). The three fit in the "basin brines and animal waste" water-type (Panno et al., 2006). In addition, the sample TRO_P7

368 presents a measurable [NO_3^-] of 54 mg/L, by opposition to the other two, both with [NO_3^-] <
369 0.01 mg/L (results not shown). Historical Br anthropogenic sources such as emissions from
370 an antiknock additive in leaded gasoline, flame retardants, dyes, pharmaceuticals or
371 pesticides in agriculture are well-known (e.g., Flury and Papritz 1993), and while some were
372 phased out, others are still in use (e.g., Shaw et al., 2010). As briefly pointed in Section 2,
373 the Lima, Sado and Mira estuaries have their specific histories of anthropogenic
374 disturbances, but the effort to better distinguish the likely detected Br^- contamination in
375 water samples (Figure 2B) is beyond the scope of the present study.

376

377 **3.2. Br–OM relationships in marsh surface environments**

378 The data gathered in the newly investigated salt marshes regarding interstitial waters (Table
379 1) are scarce due to several sampling and analytical constraints. This, together with the
380 presence of samples disturbed by anthropogenic activities frustrated our goal of broadening
381 the “evidence base” for natural [Br^-] interstitial water patterns in salt marshes. It was earlier
382 detected in the Caminha salt marsh that a pattern appears to be mainly dictated by marine
383 influence (periodic tidal flooding), i.e., higher [Br^-] in low marsh zone (average 71 mg/L;
384 Table 1), exposed to longer inundation periods by seawater and, consequently, prone to
385 greater inflow of bromide (Moreno et al., 2015). This is correlated with the relative
386 submersion times (annual basis) in the Caminha salt marsh, which is *ca.* 76–53% for tidal
387 flat, *ca.* 53–10% for low marsh and *ca.* 10–2% for the high marsh (Fatela et al., 2009).

388 Br^- entering salt marshes can be cycled by several biotic and abiotic OM bromination
389 mechanisms (e.g., Keppler et al., 2000, 2004; Hamilton, 2003; Saito and Yokouchi, 2006;
390 Wishkerman et al., 2008; Leri et al., 2010; Leri and Myneni, 2012; Leri and Ravel, 2015). All
391 include the production of an oxidized form of Br that reacts with electron-rich organic

molecules, with the subsequent formation of organobromine by-products (Leri et al., 2014). Among them, it is the highly volatile gas CH_3Br (e.g., Wuosmaa and Hager, 1990; Hamilton et al., 2003; Keppler et al., 2000, 2004; Saito and Yokouchi, 2006). Therefore, both the halophytic vegetation cover and the soil/sediment organic fraction of tidal salt marshes are the main settings and substrates for the conversion of inorganic Br (Br_{inorg}) into organic Br (Br_{org}), which can largely contribute to their Br pool (Moreno et al., 2015). It also explains why the total [Br] in (coastal) soils/sediments might not necessarily correlate with [Br^-] in water (Leri and Ravel, 2015). This lack of correlation is clear in the investigated salt marshes, where some mismatch is observed between [Br^-] in interstitial waters and the total [Br] gradient in surface soils/sediments (Tables 1 and 2; Figure 3). The highest total Br concentrations were found in the high marsh zones from Minho (average: 389 mg/kg) and Mira (avg.: 233 mg/kg) estuaries, while in their respective low marshes these contents did not exceed, on average, 133 mg/kg and 152 mg/kg (Table 2). Salt marshes from the Sado are the most depleted in both Br and OM, with average (median) values of 53 mg/kg and 8.2% (low marsh), and 81 mg/kg and 11.7% (high marsh), respectively. In the Lima estuary, Br trends are quite distinct (Table 2). This might be explained by the dominance of a coarser soil/sediment fraction (mainly sands) in the samples from these salt marshes transects (results not shown). Since a direct correlation has been well-established and widely accepted between mud (clay and/or silt) grain size fractions and both Br (e.g., Correns, 1956; Vinogradov, 1959) and OM (e.g., Buchanan and Longbottom, 1970; Mayer, 1994) contents, Br concentrations can be diluted in coarse-grained samples. The NSR_L transect is additionally impacted by a dredged sand processing facility located in the marsh surrounding area, causing resuspension of large quantities of sediment and disturbing this salt marsh (Cardoso et al., 2008).

The spatial pattern across soil/sediment surface transects (Figure 3) presents a strong direct correlation between Br and %OM (Lima: $r= 0.89$; $N= 28$; $p < 0.001$; Minho: $r= 0.86$;

N= 21; $p < 0.001$; Mira: r= 0.79; N= 29; $p < 0.001$, and Sado r= 0.67; N= 34; $p < 0.001$; tidal flat samples are also included in the computed correlation coefficients). These results are in good agreement with other studies (e.g., Cundy et al., 2005), suggesting that elevation is a key factor controlling the soil/sediment C_{org} pools of tidal salt marshes, as suggested by Spohn and Giani (2012, 2013). These authors not only have found higher C_{org} stocks in the high marsh zones with limited flooding, but a major contribution of autochthonous (in situ) OM inputs of the halophytic plant cover to soils and sediments at higher elevation within the tidal frame. Such findings could likewise enlighten the preferential total Br enrichment in the surface soils/sediments from the studied high marshes. Assuming that this Br is present mainly as organobromine, the higher concentrations found in the high marsh zones, typically characterized by greater density of stems and litter, can be associated to the relatively fast oxidation of part of Br^-, which seems to lead to a rapid conversion to Br_{org} (Leri and Myneni, 2012).

Similarly, the role of vegetation should be highlighted. The ubiquity of non-succulent perennial species (*Juncus maritimus*) in the Caminha and Lima salt marshes contrasts with the dominance of succulent species (e.g., from *Sarcocornia*/*Salicornia* genera) in Sado and Mira salt marshes. Manley et al. (2006) and Blei et al. (2010) found higher relative Br contents in succulent species, which (succulence) results from their strategy to survive in saline soils by maintaining a large amount of tissue water. According to Manley et al. (2006), high Br tissue levels would make of these succulent halophytes prolific CH_3Br producers, although suggesting that each plant species has very different intrinsic abilities to produce CH_3Br. Blei et al. (2010) showed that the variations in the Br content found on salt marsh vegetation do not explain the spatial differences in CH_3Br flux magnitudes, concluding instead that the limiting factor lies on the plants conversion mechanism (abiotic and/or biotic). Wishkerman et al. (2008) reported that the abiotic reaction (occurring between plant pectin and Br followed by CH_3Br emission) is strongly influenced by both air

444 temperatures, increasing by a factor of two for every 5ºC increase, and plants succulence,
445 becoming more efficient as plants dry out. Rhew et al. (2014) estimated that only
446 approximately 0.17% Br in the leaf tissue of *Batis maritima* L. (known as one of the CH_3Br
447 greatest producers in salt marshes) is daily removed via CH_3Br emissions, indicating that to
448 impact Br availability, a small separated subset of "*active* Br" at the enzyme site would be
449 needed. According to them, if this *active* Br pool was 0.5% of the overall tissue content, then
450 CH_3Br emissions could reduce daily that pool by 34% for Br. This ongoing discussion is of
451 major importance as it holds the power for unbalancing the total [Br^-] (either reducing or
452 increased it) available to ultimately be converted in Br_{org} in a given marsh. As a final remark
453 we would like to draw attention to the extensive intertidal habitat of *Zostera noltii* in Sado
454 and Mira estuaries (Cunha et al., 2013), and its possible impact on the Br estuarine cycling.
455 This seagrass along with *Zostera marina* Linnaeus 1753, which though very rare occurs as
456 well in the Mira estuary (Cunha et al., 2013), also have been identified as
457 producers/emitters of volatile Br compounds, such as CH_3Br and $CHBr_3$ (Weinberg et al.,
458 2013, 2015).

459 Interestingly, maximum Br soil/sediment enrichment in all studied salt marshes occurs in the
460 highest low marsh transitioning to high marsh, in the so-called upper driftline zone (Adam,
461 1990; Gerlach 1999; Persicke et al. 1999; Lefeuvre et al., 2000; Gettner, 2003). These
462 areas represent a tidal-terrestrial/freshwater transition interface, where most drift litter
463 accumulates, usually containing a high concentration of seeds and vegetative material
464 (Mineke and Bakker 2002). While this litter is effectively taken out of the estuarine
465 circulation (e.g., Boorman, 2003), it becomes potentially accessible for promoting the
466 magnification of the local C_{org} pool of soils/sediments. As a result, and even if the
467 understanding of the internal marsh processes affecting OM accumulation and turnover is
468 limited (Fagherazzi et al., 2013) – identical to the mechanisms regulating Br^- fluxes –, it
469 seems plausible to consider the upper driftline zones as promising Br_{org} sink areas, from the

standpoint of the current knowledge about OM bromination. Driftline zones might also be natural laboratories for studying the short and longer-term impacts of counterbalancing controls, like temperature, moisture and inundation (e.g., Lewis et al., 2014) as well as priming (e.g., Gontikaki et al., 2013) on OM mineralization, distressing Br sequestration and its fate in coastal environments.

Finally, the identified Br reduction in the soils/sediments collected at the highest high marsh (Figure 3) can be attributed to the increased influence of adjacent terrestrial uplands, taking into account the principle that the terrestrial environment, and thus terrestrial OM, is relatively poor in bromine (Mayer et al., 2007).

3.2. Br temporal trends in SW (Mira estuary) and NW (Minho estuary) coasts

3.2.1. Comparing Br enrichment in relation to the long-term OM storage ability from salt marshes in their soils/sediments

Casa Branca salt marsh (FWCBr core; Mira estuary) down-core profiles of Br and OM up to 89 cm depth (AD 1190) are presented in Figure 4, along with the profiles previously obtained from the Caminha salt marsh up to 62 cm depth (AD 1143) (FCPw1 core; Fig. 3 of Moreno et al., 2015). Also shown in Figure 4 are the corresponding computed Br/OM ratio trends for both cores.

The FWCBr core presents Br concentrations in the range 129–560 mg/kg while the OM content varies between 4.9% and 23.6% (Appendix B), with values uniform from the base (AD 1190) until around AD 1920 (Br: 129–215 mg/kg; average 161 ± 5 mg/kg; OM: 4.9–8.3%; average 6.7 ± 0.2%). Then, in the core's uppermost part, both Br and OM increase significantly, with two peaks at AD 1984 and AD 2010. This depth profile contrasts with the wider range and higher average Br content recorded in the FCPw1 core (Caminha):

494 average concentration of 747 mg/kg after the tidal marsh set up in AD 1330; minimum of 68
495 mg/kg, AD 1143 and maximum of 1300 mg/kg by AD 1700 (Moreno et al., 2015). It seems
496 important to mention the concomitant tidal marsh build-up in both places, as indicated by
497 the core's analysis of preserved benthic foraminifera associations: AD 1330 in Caminha
498 (Moreno et al., 2014) and AD 1323 in Casa Branca (unpublished data). This event occurs
499 during the transition from the Medieval Climatic Anomaly (MCA; 900–1300) to the LIA
500 (1350–1900) and it is likely related to the main MCA–LIA shifts in local-to-regional
501 hydroclimatic conditions in Iberian Peninsula (e.g., Lebreiro et al., 2006; Moreno et al.,
502 2012).

503 The strong direct Br–OM correlation identified in surface marsh environments is preserved
504 in the cored sediment samples with depth ($r= 0.91$; $N= 30$; $p < 0.001$), like previously
505 described for the Caminha salt marsh ($r= 0.83$; $N= 49$; $p < 0.001$). This Br–OM correlation
506 occurs independently of the large differences observed between the two cores regarding
507 their Br and OM inventories (Figure 4). Indeed, and despite the evidence provided herein
508 showing that the Mira estuary is subject to greater influence from Br^- enriched coastal
509 waters than Minho, the FWCBr core is relatively depleted in total Br (Appendix B). This
510 depletion is also true for the amounts of long-term OM storage in both salt marshes
511 soils/sediments. While in the FCPw1 core near 45% of the samples can be labelled as
512 highly organic (OM > 30%) and *ca.* 41% as organic (organic content in the 15%–30%
513 range), in the FWCBr core almost 94% of the samples can be classified as mineral soils
514 with organics (organic content > 3% and ≤ to 15%) (Huang et al., 2009). Therefore, and
515 consistent with the Br–OM relationship (leading to the production of organobromine
516 compounds) found in the surface/modern marsh habitats, it can be hypothesized that the
517 primary driver of the whole dissimilar Br pool size of these two coastal tidal marshes is their
518 technical C_{org} sink capacity, constraining the amount of C_{org} that is sequestered in each.
519 Generally, decomposition rates in salt marshes are lower than OM inputs (allochthonous

520 and autochthonous), the reason why they are recognized as one of the most powerful C_{org}
521 sinks on the planet (e.g., Macreadie et al., 2013). However, it is expected that at a regional
522 scale, soil/sediment C_{org} pools are dependent upon several decomposition rate modifiers
523 (e.g., litter chemical composition, climate, nutrient availability, communities of soil/sediment
524 organisms, and site-specific factors), creating diverse geographic patterns as regards C_{org}
525 sequestration. Among those controls, salinity seems to be a major factor, and it is
526 suggested that on tidal marshes soil C_{org} sequestration increases with decreasing salinity
527 (e.g., Poffenbarger et al., 2011; Van de Broek et al., 2016). Actually, salinity seems to have
528 an even stronger impact than elevation on the soil/sediment OM pools of tidal marshes,
529 inhibiting above-ground biomass and by enhancing OM mineralization (Hansen, 2015). In
530 the climatic context of the Mira estuary, the evapotranspiration rates usually exceed
531 precipitation, with tidal seawater supplying most of the moisture to the Casa Branca salt
532 marsh soils/sediments. This induces high salinity even on the high marsh (Table 1), with
533 Fatela et al. (2016) referring the occurrence of modern hypersaline conditions, with maxima
534 records of 48‰, in the Mira lower estuary. Foraminiferal evidence (that will be discussed
535 elsewhere) supports the idea that the (higher) Mira salinity baseline has been dominant
536 across the timeframe investigated, with assemblages dominated by *Jadammina*
537 *macrescens* (Brady, 1870) and *Trochammina inflata* (Montagu, 1808) (average 92%)
538 (unpublished data). Such high salinity baseline is, in turn, a possible explanation to the
539 lower OM in-depth concentrations from the FWCBr profile, which agrees with results from
540 other studies (e.g., Van de Broek et al., 2016 and references therein).

541 Moreover, climate has a fundamental influence on the quantity (and quality) of inputs to the
542 soil OM pool, with C_{org} stocks being largest toward cooler and wetter locations, and smallest
543 at hotter and drier regions, as established by other studies of terrestrial ecosystems (e.g.,
544 Jenny, 1941; Meentemeyer, 1978; Liu et al., 2012, and references therein). These climatic
545 gradients can have left their signature on the temporal evolution of the C_{org} storage in the

546 Caminha and Casa Branca study sites. This is revealed by their individual temporal
547 soil/sediment OM patterns, developed in response to the long-term climatic gradient
548 between the NW and SW coasts of rising temperature and decreasing precipitation (as can
549 be observed in Figure 4), with plausible direct implications on Br longer-time-scale trend, as
550 explained before.

551 The strong direct Br–OM correlation holds for both the labile ($r = 0.92$, $N = 30$; $p < 0.001$) and
552 the relatively more recalcitrant OM ($r = 0.88$; $N = 30$; $p < 0.001$) fractions from the Casa
553 Branca salt marsh soils/sediments (results not shown). This result is consistent with recent
554 investigation, in which a series of model experiments allowed to establish the existence of a
555 natural, abiotic mechanistic source both of aliphatic (more labile) and aromatic (more
556 recalcitrant) forms of Br_{org} in plant debris and humic substances in soil environment (Leri et
557 al., 2014), and marine particulate OM (Leri and Ravel, 2015). The soil humic substances
558 showed a recalcitrant aromatic Br_{org} speciation, leading Leri et al. (2014) to suggest that this
559 might provide a useful proxy for evaluating the rate of OM burial in sediments. In this
560 direction, is worth mentioning the work by Biester et al. (2004, 2006) and Martínez-Cortizas
561 et al. (2007, 2016) in peatland soils, where they have started to study the temporal trends of
562 the more stable Br_{org} compounds and the role of the main pedogenetic processes on Br
563 accumulation. Altogether, this analysis can help future research on the Br–OM link in tidal
564 marshes, needed to support the use of Br in marsh soils/sediments as a paleoclimatic
565 indicator.

566 Finally, we propose a conceptual model for the salt marshes Br cycle in our case study
567 (Caminha and Casa Branca) in order to summarize the interplay between the forcing factors
568 analysed along the lines of the previous discussion. The interactions illustrated in Figure 5
569 are, in our view, the most likely to have a strong influence on salt marshes short and even
570 longer-term role to act as a source and/or as a sink for Br. Accordingly, NW coast high

571 marshes under the sustained influence of concomitant lower photosynthetically active
572 radiation (PAR), corresponding to the spectral range of solar radiation from 400 to 700 nm
573 that is used in photosynthesis reactions (e.g., Mariscal et al., 2000), and colder wetter
574 conditions developed lower salinity baselines where the vegetation cover largely consists of
575 non-succulents. These lower salinity (mesohaline) tidal marshes have typically higher rates
576 of plant productivity and lower decomposition rates of dead and senescing plant material,
577 leading to higher accumulation of soil/sediment OM (e.g., Morrisey et al., 2014).
578 Collectively, these processes culminate in lesser CH_3Br atmospheric emissions from
579 marshes and higher Br_{org} concentration in their soils/sediments. On the other hand, the SW
580 coast high marshes, settled under higher available PAR conditions and a hotter and dryer
581 climate, show a higher (polyhaline to euhaline) salinity baselines and consequently lower
582 productivity, being mostly colonized by succulent plants more adapted to saline conditions
583 and greater emitters of CH_3Br. These conditions finally lead to a lower long-term storage of
584 OM and Br_{org} in soils/sediments.

585 The afore-described model establishes a connection with the analysis of the Br temporal
586 variability in light of the past SA–climate link made in the next section.

587

588 *3.2.2. Br enrichment peaks in association with Grand Minima of solar activity*

589 The manifestation of a solar activity (SA) Grand Minima in terrestrial climate has been well
590 established after the pioneering work of Eddy (1976). The most recent Grand Minima in
591 reconstructed SA, as expressed by the TSI variation (Steinhilber et al., 2012), are presented
592 in Figure 4 (Maunder Minimum – MM; 1645–1715; Spörer Minimum – SM; 1450–1550; and
593 Wolf Minimum – WM; 1282–1342). Note that the Dalton Minimum (DM; 1790–1820) has a

distinct physical origin (Duhau and de Jager (2010), and it is therefore not regarded today as a Grand Episode of SA.

In the last few decades, extensive research work has been done towards a better understanding of the Sun-Earth's climate coupling system, with great progress being achieved (e.g., Haigh, 2007; Soon et al., 2014 for a review). Recently, Brugnara et al. (2013) referred that the Euro–Atlantic sector, in which Portugal is located, seems to be a region with a particularly strong solar influence on the troposphere, finding a weak but significant change in the mean late winter circulation over Europe, which culminates in detectable impacts on the near-surface climate. The results obtained by Jiang et al. (2015) suggest not only that climate in the northern North Atlantic regions follows SA fluctuations on multidecadal to centennial time scales, but also that it is more susceptible to the influence of those fluctuations throughout cool periods with, for instance, less vigorous ocean circulation. Similar results were found by Gómez-Navarro et al. (2012) in the context of climate simulations for the second millennium over the Iberian Peninsula. These researchers studied the impact of natural forcing and internal variability on climate, and found that temperature and precipitation variability are significantly affected at centennial scales by variations in the SA.

Grand Minima and Dalton-type Minimum scenarios are broadly characterized by (i) lower TSI (i.e., lower available PAR) (Lean, 1991, and references therein), (ii) development of cloudiness (e.g., Usoskin and Kovaltsov, 2008), and (iii) decreased global/regional air surface temperatures (e.g., Neukom et al., 2014) in tandem with greater regional precipitation variability. In the Iberian Peninsula, according with the modelled results from Gómez-Navarro et al. (2011), precipitation could have increased in response to reduced solar forcing (Figure 4), prompting greater river discharges. Also Cruz et al. (2015) related maxima rainfall episodes, as recognized in their stalagmite record, with other Grand Solar

619 Minima, suggesting a strong coupling between SA and precipitation over northern Iberia,
620 which agrees with Gómez-Navarro et al. (2012) outcomes in the context of climate
621 simulations.

622 Up to now, and in the absence of a “unified hypothesis”, the explanations for the
623 connections between solar phenomena and the lower atmosphere processes can be
624 summarized in two types of mechanisms: (i) “top-to-down”, influencing the pole-to-equator
625 temperature gradient and exerting an impact on the modulation of the atmospheric
626 circulation cells, weakening or strengthening the zonal winds, and (ii) “bottom-to-up” that
627 directly impact on the radiation fluxes, energy balance and temperatures on the ground.
628 Depending on the surface albedo a part of this radiation is absorbed and transformed into
629 latent or sensible heat. During periods of lower SA, less radiation is available in the tropics
630 for conversion to latent heat, which is thought to lead to a weakening of the Hadley and
631 Ferrel cells (Labitzke et al., 2002). Other than intensity, the position and extent of those cells
632 are also affected, inducing latitudinal shifts. Hence both mechanisms finally impact the
633 atmospheric circulation modes responsible for the global/regional precipitation and
634 temperature patterns (e.g., Gray et al., 2010; Martin-Puertas et al., 2012; Thiéblemont et al.,
635 2015).

636 Therefore, if solar variations are an important source of regional climate variability, we might
637 expect that paleoclimate proxies reproduce somewhat the climatic response to SA changes.
638 In line with this, Moreno et al. (2015) suggested that Br soil/sediment enrichment in the
639 Caminha salt marsh (NW coast) is, at least partially, related to the SA pattern over the last
640 almost 800 years. This can be extended to Casa Branca salt marsh (SW coast), essentially
641 through a SA control on (i) available PAR fluctuations and (ii) regional temperature and
642 precipitation regimes, affecting evapotranspiration rates and, as a result, interstitial water
643 salinity at the upper elevations within the marsh. Indeed, the relationship between the

curves presented in Figure 4 is clear, with periods of highest Br enrichment (FCPw1 and FWCBr) agreeing with major excursions in SA. This means that the TSI negative anomalies (Steinhilber et al., 2012) from the Dalton, Maunder, Spörer and Wolf Solar Minima, to which correspond periods of both modelled lower temperature and increased precipitation in the NW and SW of Portugal (Gómez-Navarro et al., 2011), are marked by Br positive peaks in marshes soils/sediments, more clearly observed in Br/OM ratio curves to account for changes in OM content (see black arrows). Considering only the group of samples from the FWCBr core falling within the LIA (with stronger impacts on the climate of Europe and other regions neighbouring the North Atlantic during the 16th–19th centuries; e.g., Mann, 2002), three display a more pronounced Br excess relative to OM, lying outside the upper 95% confidence limit of their linear regression interval: AD 1451 (Spörer Minimum), and AD 1694 and AD 1660 (both in the Maunder Minimum). These sedimentary records, considered altogether with other climatic proxies for the NW of Portugal (Moreno et al., submitted), strongly suggest that the LIA resulted in a wetter and cool climate in this south-western European region, triggering major hydrological changes present in paleoecological records, namely from high marsh benthic foraminifera (Moreno et al., 2014). Specifically, climatic shifts driven by Grand Minima on western Portuguese coast could have forced a deceleration of the whole dynamics involving the net CH_3Br phytogenic emissions to the atmosphere, thus favouring Br sequestration and storage (as Br_{org}) in marsh soils/sediments. Throughout SA Grand Minima (↓TSI/PAR), the climate controls departed from normal values (↓T; ↓ET; ↑P; see Figure 5), inducing a decrease in marsh interstitial salinity, certainly ended in higher plant productivity peaks (e.g., De Leeuw et al., 1990), thereby causing a rise in salt marsh sediment C_{org} accumulation over time, with plant debris more enriched in Br and liable to further bromination during the humification process.

Rhew et al. (2014) emphasized that CH_3Br phytogenic emissions from coastal salt marshes, present a dramatic inter- and intra-marshes variability, namely in relation to magnitude

(subtropical salt marshes showing much higher emission rates than temperate salt marshes) and seasonality. They recorded maxima CH_3Br emission fluxes in peak summer growing season (July) and lowest at the end of the growing season (November). The latter were registered during the morning and coincident with the high tide. They also found a pronounced mid-day peak, coinciding with the time of highest ambient air and surface soil temperatures, in the diurnal CH_3Br emission trend, with this one mirroring the variation of PAR.

Considering both CH_3Br phytogenic emissions and the ubiquity of soil/sediment OM bromination, and applying them to a Grand Minima scenario (↓TSI/available PAR; ↓air surface temperatures; ↓growing seasons, ↑rainfall leading to ↑soil/sediment saturation), a reliable framework for the Br enrichment in temperate marsh habitats triggered by climatic shifts driven by SA can be proposed (see Figure 5), recognizing that further work would be required to completely prove this assumption.

Volcanic eruptions may also represent an alternative source of Br to salt marshes during Grand Minima Episodes (see Figure 4). The first discovery of volcanic BrO (Bobrowski et al., 2003), and its subsequent measurement in many volcanic plumes around the globe (e.g., Roberts et al., 2014) demonstrates the formation of reactive bromine (firstly as Br_2, which then converts into other forms including Br, BrO, HOBr, $BrONO_2$) during these events, which can be removed (at least partially) from gaseous phase by aerosol, water and ice-uptake (followed by particle sedimentation) (Fernandez et al., 2014; Jourdain et al., 2015). Reactive bromine acts as a catalyst to its own formation, leading to an exponential growth called “bromine explosion”. The LIA Grand Minima have been punctuated by considerable volcanic activity (e.g., D’Arrigo et al., 2013; Figure 4). D’Arrigo et al. (2013) highlighted, as two of the major volcanic events over the past millennium, the eruptions of AD 1453 (Kuwae Volcano, Vanuatu; Spörer Minimum) and AD 1815 (Mount Tambora,

Indonesia; Dalton Minimum). Such episodes of great volcanic activity and their worldwide effects (e.g., Trigo et al., 2009; Koffman et al., 2013) might also have had the potential for causing disruption on the Br cycling in Caminha and Casa Branca salt marshes, contributing somewhat for their soils/sediments Br enrichment throughout Grand Minima.

4. Conclusions

The present study addresses major topics concerning the Br cycling in contrasting salt marshes environments of four western Portuguese estuaries – Minho, Lima, Sado and Mira, drawing attention for its complexity and linkages with OM dynamics. We provided evidence that besides the marine influence, Br enrichment of these marshes is ultimately connected to their ability for long-term C_{org} storage. A clear difference between the marshes from NW and SW coasts stands out, with the former being more enriched in both OM and total Br. This contrasting behaviour is driven by different climatic conditions between the two regions that favour more strongly the mechanisms and processes of OM production, burial, and preservation (with concomitant incorporation of Br) in the north-western coastal salt marshes, in contrast with the SW coast, most probably as a result of the higher salinity (lesser productivity) of the latter. Seemingly, this same NW climatic setting inhibits the emission of comparatively larger phytogenic CH_3Br fluxes to atmosphere. This might be intensified as a result of the marshes colonization by non-succulent species (less efficient in the CH_3Br production), further promoting the Br enrichment of soil/sediment OM.

Although the applied approach is constrained by chronological uncertainties, cores sampling resolution or the (relatively short) time series lengths, preventing the application of enhanced methodologies in the time-frequency domain, the Br temporal variability in the Caminha and Casa Branca salt marshes can be related to SA oscillations, showing greater

719 Br enrichment during Grand Minima or Minima-like Episodes. This can be explained in
720 connection with the changing temperature (decrease) and precipitation (increase) regimes
721 in the NW and SW coasts of Portugal induced by lower TSI (available PAR), as pointed out
722 by previous studies and supported by climate simulations. The contribution of major tropical
723 volcanic explosions at Grand Solar Minima during the registered higher Br enrichment in the
724 two Portuguese salt marshes is also considered.

725 Finally, we expect that the issues encompassed here can be deepened in future research
726 about the Br biogeochemical cycle in salt marshes worldwide. The proposed conceptual
727 framework identifies several influences capable of imbalance the Br–OM interconnections
728 and helps to prioritize which are likely to play key roles on salt marshes Br recycling, in
729 order to improve, henceforward, its reliability as a marker of climate change driven by past
730 SA. In line with this, it is important to bear in mind that for robustly test solar-climate signals
731 in Br tidal salt marsh records, large and widespread ensembles of well-dated data are
732 required along with high-resolution sampling.

733

734 **Acknowledgements**

735 This work was partly supported by IDL through the UID/GEO/50019/2013 program, by C^2TN
736 through the UID/Multi/04349/2013 program, and is a contribution of the project WestLog
737 (PTDC/CTE/105370/2008), funded by the Fundação para a Ciência e a Tecnologia (FCT).
738 João Moreno benefits from a FCT PhD grant (SFRH/BD/ 87995/2012). The authors would
739 like to express their sincere gratitude to Inês Pereira, Ana Medeiros and Vera Lopes for
740 carrying out the soils and sediments geochemical analysis, and the proof-reader Carla
741 Neves. J.J. Gómez-Navarro acknowledges the funding provided through the contract for the
742 return of experienced researches, resolution R-735/2015 of the University of Murcia.

References

Adam, P., 1990. Salt marsh ecology. Cambridge University Press, Cambridge, UK, 461p.

Adams, S.S., 1969. Bromine in the Salado Formation, Carlsbad Potash District, New Mexico. State Bureau of Mines and Mineral Resources, Bulletin 93, Socorro, New Mexico, 122 p.

Adolphi, F. and Muscheler, R., 2016. Synchronizing the Greenland ice core and radiocarbon timescales over the Holocene – Bayesian wiggle-matching of cosmogenic radionuclide records. Climate of the Past 12, 15–30.

Alcalá, F.J. and Custodio, E., 2008. Using the Cl/Br ratio as a tracer to identify the origin of salinity in aquifers in Spain and Portugal; Journal of Hydrology 359, 189–207.

Almeida, C.M.R., Mucha, A.P. and Vasconcelos, M.T., 2011. Role of different salt marsh plants on metal retention in an urban estuary (Lima estuary, NW Portugal). Estuarine, Coastal and Shelf Science 91, 243–249.

Alves, A.M.C., 2003. O estuário do rio Lima: pressão antrópica e caracterização ambiental. Ciências da Terra (UNL), Lisboa, special nº. V, CD-ROM, pp. H5–H9.

Amaral, V., Queiroga, H., Skov, M. and Paula, J., 2007. Planktonic availability and settlement of *Carcinus maenas* megalopae at high temporal resolution in the lower Mira Estuary (SW Portugal). Marine Ecology Progress Series 348, 239–248.

APA, 2011. Sistema Nacional de Informação de Ambiente da Agência Portuguesa do Ambiente (SNIAmb).http://sniamb.apambiente.pt/.

Appleby, P.G., 2001. Chronostratigraphic techniques in recent sediments. *In* W.M. Last, J.P. Smol (Eds.), Tracking Environmental Change Using Lake Sediments, 1. Dordrecht, The Netherlands: Kluwer Academic Publishers, p. 171–203.

Appleby, P.G. and Oldfield, F., 1978. The calculation of lead-210 dates assuming a constant rate of supply of unsupported ^{210}Pb to the sediment. Catena 5, 1–8.

Araújo, M.F., Valério, P. and Jouanneau, J-M., 1998. Heavy metal assessment in sediments of the Ave river basin (Portugal) by EDXRF. X-Ray Spectrometry 27, 305–312.

Araújo, M.F., Conceição, A., Barbosa, T., Lopes, M.T. and Humanes, H. 2003. Elemental composition of marine sponges from the Berlengas Natural Park, Western Portuguese Coast. X-Ray Spectrometry 32, 428–433.

Azevedo, I., Ramos, S., Mucha, A.P. and Bordalo, A.A., 2013. Applicability of ecological assessment tools for management decision-making: A case study from the Lima estuary (NW of Portugal). Ocean & Coastal Management 72, 54–63.

Bettencourt, A., Ramos, L., Gomes, V., Dias, J.M.A., Ferreira, G., Silva, M. and Costa, L., 2003. Estuários Portugueses. Ed. INAG – Ministério das Cidades, Ordenamento do Território e Ambiente, Lisboa, 311 p.

795 Biester, H., Keppler, F., Putschew, A., Martínez-Cortizas and Petri, M., 2004. Halogen
796 retention, organohalogens, and the role of organic matter decomposition on halogen
797 enrichment in two Chilean peat bogs. Environmental Science & Technology 38, 1984–1991.
798
799 Biester, H., Selimović, D., Hemmerich, S., and Petri, M., 2006. Halogens in pore water of
800 peat bogs – the role of peat decomposition and dissolved organic matter. Biogeosciences 3,
801 53–64.
802
803 Blei, E., Heal, M.R. and Heal, K.V., 2010. Long-term CH_3Br and CH_3Cl flux measurements
804 in temperate salt marshes. Biogeosciences 7, 3657–3668.
805
806 Bobrowski, N., Hönninger, G., Galle, B. and Platt, U., 2003. Detection of bromine monoxide
807 in a volcanic plume, Nature, 423, 273–276.
808
809 Boorman, L.A., 2003. Saltmarsh Review. An overview of coastal saltmarshes, their dynamic
810 and sensitivity characteristics for conservation and management. JNCC Report, No. 334,
811 113p.
812
813 Bridgham, S.D., Megonigal, J.P., Keller, J.K., Bliss, N.B. and Trettin, C., 2006. The carbon
814 balance of North American wetlands. Wetlands 26, 889–916.
815
816 Brugnara, Y., Brönnimann, S., Luterbacher, J. and Rozanov, E., 2013. Influence of the
817 sunspot cycle on the Northern Hemisphere wintertime circulation from long upper-air data
818 sets. Atmospheric Chemistry and Physics 13, 6275–6288.
819

820 Buchanan, J.B. and Longbottom, M.R., 1970. The determination of organic matter in marine
821 muds: the effect of the presence of coal and the routine determination of protein. Journal of
822 Experimental Marine Biology and Ecology 5, 158–169.
823
824 Cardoso, R., Araújo, M.F., Freitas, M.C. and Fatela, F., 2008. Geochemical characterisation
825 of sediments from marginal environments of Lima Estuary (NW Portugal). e-Terra, Revista
826 Electrónica de Ciências da Terra Volume 5 – Nº 6, GEOTIC – Sociedade Geológica de
827 Portugal, 11 p.
828
829 Carpenter, L.J. and Reimann, S. (Lead Authors), Burkholder, J.B., Clerbaux, C., Hall, B.D.,
830 Hossaini, R., Laube, J.C., and Yvon Lewis, S.A., 2014. Ozone-Depleting Substances
831 (ODSs) and Other Gases of Interest to the Montreal Protocol. Chapter 1 in Scientific
832 Assessment of Ozone Depletion: 2014, Global Ozone Research and Monitoring Project-
833 Report Nº 55, World Meteorological Organization, Geneva, Switzerland.
834
835 Castro, P. and Freitas, H., 2006. Anthropogenic effects and salt marsh loss in the Mondego
836 and Mira estuaries (Portugal). Web Ecology 6, 59–66.
837
838 Chipperfield, M.P., 2015. Global Atmosphere – The Antarctic Ozone Hole. *In* Still Only One
839 Earth: Progress in the 40 Years since the First UN Conference on the Environment, 2015,
840 pp. 1–33.
841
842 Correns, C.W., 1956. The Geochemistry of Halogens. *In* L.H. Ahrens, K. Rankama and S.K.
843 Rancorn (Eds.), Physics and Chemistry of the Earth, Vol. 1, Pergamon Press, New York,
844 pp. 181–233.
845

Costa, M.J. Catarino, F. and Bettencourt, A., 2001. The role of salt marshes in the Mira estuary (Portugal). Wetlands Ecology and Management 9, 121–134.

Costa, J.C., 2001. Tipos de vegetação e adaptações das plantas do litoral de Portugal continental. *In* M.E. Albergaria Moreira, A. Casal Moura, H.M. Granja and F. Noronha (Eds.) Homenagem (in honorio) Professor Doutor Soares de Carvalho. Universidade do Minho, Braga, pp. 283–299.

Costa, J.C., Arsénio, P., Monteiro-Henriques, T., Neto, C., Pereira, E., Almeida, T. and Izco, J., 2009. Finding the boundary between Eurosiberian and Mediterranean salt marshes. Journal of Coastal Research SI 56, 1340–1344.

Costa-Dias, S., Ronaldo Sousa, R. and Antunes, C., 2010. Ecological quality assessment of the lower Lima Estuary. Marine Pollution Bulletin 61, 234–239.

Cox, M.L., Fraser, P.J., Sturrock, G.A., Siems, S.T. and Porter, L.W., 2004 Terrestrial sources and sinks of halomethanes near Cape Grim, Tasmania. Atmospheric Environment 38, 3839–3852.

Crowley, T.J., 2000. Causes of climate change over the past 1000 years. Science 289, 270–277.

Cruz, J.A., Turrero, M.J., Cáceres, J.O., Marín-Roldán, A., Ortega, A.I., Garralón, A., Sánchez. L., Gómez, P., Munõz-García, M.B., Edwards, R.L. and J. Martín-Chivelet, J., 2015. Long-term hydrological changes in northern Iberia (4.9–0.9 ky BP) from speleothem

871 Mg/Ca ratios and cave monitoring (Ojo Guarenã Karst Complex, Spain) Environmental
872 Earth Sciences 74, 7741–7753.
873
874 Cundy, A.B., Hopkinson, L., Lafite, R., Spencer, K., Taylor, J.A., Ouddane, B., Heppell,
875 C.M., Carey, P.J., Charman, R.O., Shell, D., Ullyott, J.S., 2005. Heavy metal distribution
876 and accumulation in two Spartina sp.-dominated macrotidal salt marshes from the Seine
877 estuary (France) and the Medway estuary (UK). Applied Geochemistry 20, 1195–1208.
878
879 Cunha, A.H., Assis, J.F. and Serrão, E.A., 2013. Seagrasses in Portugal: a most
880 endangered marine habitat. Aquatic Botany 104, 193–203.
881
882 D'Arrigo, R., Wilson, R. and Anchukaitis, K.J., 2013. Volcanic cooling signal in tree ring
883 temperature records for the past millennium. Journal of Geophysical Research:
884 Atmospheres 118, 1–11.
885
886 De Leeuw, J., Olff, H. and Bakker, J.P., 1990. Year-to-year variation in peak above-ground
887 biomass of six salt-marsh angiosperm communities as related to rainfall deficit and
888 inundation frequency. Aquatic Botany 36, 139–151.
889
890 Dimmer, C.H., Simmonds, P.G., Nickless, G. and Nickless, M.R., 2000. Biogenic fluxes of
891 halomethanes from Irish peatland ecosystems. Atmospheric Environment 35, 321–330.
892
893 Doff, D.H., 1989. Determination of bromine and iodine in four marine sediment reference
894 samples by Energy-Dispersive X-Ray Fluorescence Spectrometry. Geostandards
895 Newsletter 13, 75–77.
896

Drewer, J., Heal, M.R., Heal, K.V. and Smith, K.A., 2006. Temporal and spatial variation in methyl halide flux from a salt marsh. Geophysical Research Letters 33, L16808, 5 p.

Duhau, S., and De Jager, C., 2010. The forthcoming Grand Minimum of solar activity, Journal of Cosmology 8, 1983-1999.

Eddy, J.A., 1976. The Maunder Minimum. Science 192, 1189–1202.

Fagherazzi, S., Wiberg, P.L., Temmerman, S., Struyf, E., Zhao, Y. and Raymond, P.A., 2013. Fluxes of water, sediments, and biogeochemical compounds in salt marshes. Ecological Processes 2, 1–16.

Fatela, F., Moreno, J. and Cabral, M.C., 2016. Salinity and temperature water assessment of the tidal marshes from the W Portuguese coast, as an ecological tool to palaeoenvironmental reconstructions based on foraminifera and ostracoda assemblages. Estudos do Quaternário, 14, http://www.apeq.pt/ojs/index.php/apeq.

Fatela, F., Moreno, J., Moreno, F., Araújo, M.F., Valente, T., Antunes, C., Taborda, R., Andrade, C., Drago, T., 2009. Environmental constraints of foraminiferal assemblages distribution across a brackish tidal marsh (Caminha, NW Portugal). Marine Micropaleontology 70, 70–88.

Fatela, F., Moreno, J. and Antunes, C., 2007. Salinity influence on foraminiferal tidal marsh assemblages of NW Portugal: an anthropogenic constraint? Thalassas 23, 51–63.

922 Fernandez, R.P., Salawitch, R.J., Kinnison, D.E., Lamarque, J.-F. and Saiz-Lopez, A., 2014.
923 Bromine partitioning in the tropical tropopause layer: implications for stratospheric injection.
924 Atmospheric Chemistry and Physics 14, 13391–13410.
925
926 Ferreira, J.G., Simas, T., Nobre, A., Silva, M.C., Shifferegger, K. and Lencart-Silva, J.,
927 2003. Identification of sensitive areas and vulnerable zones in transitional and coastal
928 Portuguese systems. INAG, Lisboa, 151 p.
929
930 Flury, M. and Papritz, A., 1993. Bromide in the natural environment: occurrence and toxicity.
931 Journal of Environmental Quality 22, 747–758.
932
933 Gerlach, A., 1999. Winter driftline debris on the Wadden Island of Mellum, Germany;
934 distribution, quantity and decomposition. Abhandlungen Naturwissenschaftliches Verein
935 Bremen 44, pp. 707–724.
936
937 Gerritse, R.G. and George, R., 1988. The role of soil organic matter in the geochemical
938 cycling of chloride and bromide. Journal of Hydrology 101, 83–95.
939
940 Gettner, S., 2003. Untersuchungen des Zusammenhangs zwischen Treibselmengen und
941 Vorlandnutzung an der Westküste Schleswig-Holsteins. Kieler Notizen Pflanzenkunde
942 Schleswig Holstein Hamburg 31, pp. 57–71.
943
944 Gómez-Navarro, J.J., Montávez, J.P., Jiménez-Guerrero, P., Jerez, S., Lorente-Plazas, R.,
945 González-Rouco, J.F. and Zorita, E., 2012. Internal and external variability in regional
946 simulations of the Iberian Peninsula climate over the last millennium. Climate of the Past 8,
947 25–36.

948

949 Gómez-Navarro, J.J., Montávez, J.P., Jerez, S., Jiménez-Guerrero, P., Lorente-Plazas, R.,
950 González-Rouco, J.F. and Zorita, E., 2011. A regional climate simulation over the Iberian
951 Peninsula for the last millennium. Climate of the Past 7, 451–472.

952

953 Gontikaki, E., Thornton, B., Huvenne, V.A.I. and Witte, U., 2013. Negative priming effect on
954 organic matter mineralisation in NE Atlantic slope Sediments. PLoS ONE 8(6): e67722, 9 p.

955

956 Gray, L.J, Beer, J., Geller, M., Haigh, J.D., Lockwood, M., Matthes, K., Cubasch, U.,
957 Fleitmann, D., Harrison, G., Hood, L., Luterbacher, J., Meehl, G.A., Shindell, D., van Geel,
958 B. and White, W. 2010. Solar influences on climate. Reviews of Geophysics 48, RG4001,
959 53 p.

960

961 Haigh, J.D., 2007. The sun and the earth's climate. Living Review Solar Physics 4, 1e64
962 (Online article). Available at: http://www.livingreviews.org/lrsp-2007-2 (accessed
963 08.05.2016).

964

965 Hamilton, J., McRoberts W., Keppler, F., Kalin, R. and Harper, D., 2003. Chloride
966 methylation by plant pectin: An efficient environmentally significant process, Science 301,
967 206–209.

968

969 Hansen, K., 2015. Ecosystem functions of tidal marsh soils of the Elbe estuary. Dissertation,
970 Fachbereich Geowissenschaften, Universität Hamburg, Hamburger Bodenkundliche
971 Arbeiten 76, XX + 161p.

972

973 Hardacre, C.J. and Heal, M.R., 2013. Characterization of methyl bromide and methyl
974 chloride fluxes at temperate freshwater wetlands. Journal of Geophysical Research:
975 Atmospheres 118, 977–991.
976
977 Hardacre, C.J., Blei, E. and Heal, M.R., 2009. Growing season methyl bromide and methyl
978 chloride fluxes at a sub-arctic wetland in Sweden. Geophysical Research Letters 36,
979 L12401, 5 p.
980
981 Haslett, J. and Parnell, A., 2008. A simple monotone process with application to
982 radiocarbon-dated depth chronologies. Applied Statistics 57, 399–418.
983
984 Herbst, K., Heber, B., Beer, J. and Tylka, A.T., 2015. Modelling the Production of
985 Cosmogenic Radionuclides due to galactic and solar cosmic rays. The 34th International
986 Cosmic Ray Conference, PoS (ICRC2015) 537, 8p.
987
988 Honrado, J., Alves, P., Alves, H.N., Torres, J. and Caldas, F.B., 2004. A Flora e a
989 vegetação do Minho internacional – Diversidade, ecologia e valor para conservação.
990 Melgaço, Portugal: Atas do Congresso Internacional Sobre o Rio Minho; 5p.
991
992 Hu, L., Yvon-Lewis, S.A., Liu, Y., Salisbury, J.E. and O'Hern, J.E., 2010. Coastal emissions
993 of methyl bromide and methyl chloride along the eastern Gulf of Mexico and the east coast
994 of the United States. Biogeochemical Cycles 24, GB1007, 10 p.
995
996 Huang, P.-T., Patel, M., Santagata, M.C., and Bobet, A., 2009. Classification of organic
997 soils. FHWA/IN/JTRP-2008/2. Purdue University, 170 p.
998

Hurrell, J., 1995. Decadal trends in the North-Atlantic Oscillation: regional temperatures and precipitation. Science 269, 676–679.

Hurrell, J. and van Loon, H., 1997. Decadal variations in climate associated with the North Atlantic Oscillation. Climatic Change 36, 301–336.

Jenny, H., 1941. Factors of Soil Formation - A System of Quantitative Pedology. Dover Publications, Inc., New York, 291 p.

Jiang, H., Muscheler, R., Björck, S., Seidenkrantz, M.-S., Olsen, J., Sha, L., Sjolte, J., Eiríksson, J., Ran, L., Knudsen, K.-L., and Knudsen, M.F., 2015. Solar forcing of Holocene summer sea-surface temperatures in the northern North Atlantic. Geology doi:10.1130/G36377.1.

Jones, F., Vengosh, A., Rosenthal, E., Yechieli, Y., 1999. Geochemical investigation of groundwater quality. In: Proceeding: Seawater Intrusion in Coastal Aquifers - Concepts, Methods and Practices. Kluwer Academic, Dordrecht, pp. 51–71.

Jourdain, L., Roberts, T.J., Pirre, M. and Josse, B., 2015. Modeling the reactive halogen plume from Ambrym volcano and its impact on the troposphere with the CCATT-BRAMS mesoscale model. Atmospheric Chemistry and Physics Discuss. 15, 35313–35381.

Katz, B.G., Eberts, S.M. and Kauffman, L.J., 2011. Using Cl/Br ratios and other indicators to assess potential impacts on groundwater quality from septic systems: A review and examples from principal aquifers in the United States. Journal of Hydrology 397, 151–166.

Keene, W.C., Stutz, J., Pszenny, A.A.P., Maben, J.R., Fischer, E.V., Smith, A.M., von Glasow, R., Pechtl, S., Sive, B.C. and Varner, R.K., 2007. Inorganic chlorine and bromine in coastal New England air during summer. Journal of Geophysical Research 112, D10S12, 15 p.

Keller, J.K., Bauers, A.K., Bridgham, S.D., Kellogg, L.E. and Iversen, C.M., 2006. Nutrient control of microbial carbon cycling along an ombrotrophic-minerotrophic peatland gradient, Journal of Geophysical Research 111, G03006, 14 p.

Keppler, F., Eiden, R., Niedan, V., Pracht, J., and Scholer, H.F., 2000. Halocarbons produced by natural oxidation processes during degradation of organic matter, Nature 403, 298–301.

Keppler, F., Kalin, R.M., Harper, D.B., McRoberts, W.C. and Hamilton, J.T.G., 2004. Carbon isotope anomaly in the major plant C1 pool and its global biogeochemical implications, Biogeosciences 1, 123–131.

Koffman, B.G., Kreutz, K.J., Kurbatov, A.V. and Dunbar, N.W., 2013. Impact of known local and tropical volcanic eruptions of the past millennium on the WAIS Divide microparticle record. Geophysical Research Letters 40, 4712–4716.

Koh, D.-C., Mayer, B., Lee, K.-S. and Ko, K.-S., 2010. Land-use controls on sources and fate of nitrate in shallow groundwater of an agricultural area revealed by multiple environmental tracers. Journal of Contaminant Hydrology 118, 62–78.

1050 Kristensen, E., 1990. Characterization of biogenic organic matter by stepwise
1051 thermogravimetry (STG). Biogeochemistry 9, 135–159.
1052
1053 Labitzke, K., Austin, J., Butchardt, N., Knight, J., Takahashi, M., Nakamoto, M., Nagashima,
1054 T., Haigh, J., and Williams, V., 2002. The global signal of the 11-year solar cycle in the
1055 stratosphere: observations and models, Journal of Atmospheric and Solar-Terrestrial
1056 Physics 64, 203–210.
1057
1058 Lal, D. and Peters, B., 1967. Cosmic ray produced radioactivity on the Earth. *In* K. Sitte
1059 (Ed.), Handbuch der Physic / Encyclopedia of Physics, vol. 9 / 46 / 2, Springer-Verlag,
1060 Berlin, pp. 551–612.
1061
1062 Lean J., 1991. Variations in the sun's radiative output. Reviews of Geophysics 29, 505–535.
1063
1064 Lebreiro, S.M., Francés, S.G., Abrantes, F.F.G., Diz, P., Bartels-Jónsdóttir, H.B.,
1065 Stroynowski, Z.N., Gil, I.M., Pena, L.D., Rodrigues, T., Jones, P.D., Nombela, M.A., Alejo, I.,
1066 Briffa, K.R., Harris, I. and Grimalt, J.O., 2006. Climate change and coastal hydrographic
1067 response along the Atlantic Iberian margin (Tagus Prodelta and Muros Ría) during the last
1068 two millennia. The Holocene 16, 1003–1015.
1069
1070 Lefeuvre, J.-C., Bouchard, V., Feunteun, E., Grare, S., Laffaille, P. and Radureau, A., 2000.
1071 European salt marshes diversity and functioning: the case study of the Mont Saint-Michel
1072 bay, France. Wetland Ecology and Management 8, 147–161.
1073

1074 Leorri, E., Freitas, M.C., Zourarah, B., Andrade, C., Mellas, S., Cruces, A., Griboulard, R.
1075 and Lopes, V., 2010. Multiproxy approach to characterize an overwash deposit: Oualidia
1076 lagoon (Moroccan Atlantic coast). GEOGACETA 48, 7–10.
1077
1078 Leri, A.C. and Ravel, B., 2015. Abiotic bromination of soil organic matter. Environmental
1079 Science & Technology 49, 13350–13359.
1080
1081 Leri, A.C., Mayer, L.M., Thornton, K.R. and Ravel, B., 2014. Bromination of marine
1082 particulate organic matter through oxidative mechanisms. Geochimica et Cosmochimica
1083 Acta 142, 53–63.
1084
1085 Leri, A.C. and Myneni, S.C.B., 2012. Natural organobromine in terrestrial ecosystems.
1086 Geochimica and Cosmochimica Acta 77, 1–10.
1087
1088 Leri, A.C., Hakala, J.A., Marcus, M.A., Lanzirotti, A., Reddy, C.M. and Myneni, S.C.B., 2010.
1089 Natural organobromine in marine sediments: new evidence of biogeochemical Br cycling.
1090 Global Biogeochemical Cycles 24, GB4017, 15 p.
1091
1092 Lewis, D.B., Brown, J.A. and Jimenez, K.L., 2014. Effects of flooding and warming on soil
1093 organic matter mineralization in *Avicennia germinans* mangrove forests and *Juncus*
1094 *roemerianus* salt marshes. Estuarine, Coastal and Shelf Science 139, 11–19.
1095
1096 Lima, I., Moreira, S.M., Osten, JR.-V., Soares, A.M.V.M. and Guilhermino, L., 2007.
1097 Biochemical responses of the marine mussel *Mytilus galloprovincialis* to petrochemical
1098 environmental contamination along the North-western coast of Portugal. Chemosphere 66,
1099 1230–1242.

Liu, Z.P., Shao, M.A. and Wang, Y.Q., 2012. Large-scale spatial variability and distribution of soil organic carbon across the entire Loess Plateau, China. Soil Research 50, 114–124.

Macreadie, P.I., Hughes, A.R. and Kimbro, D.L., 2013. Loss of “blue carbon” from coastal salt marshes following habitat disturbance. PLoS ONE 8, e69244, 8 p.

Mahn, C.L. and Gieskes J.M., 2001. Halide systematics in comparison with nutrient distributions in sites 1033B and 1034B, Saanich Inlet: ODP Leg 169S. Marine Geology 174, 323–339.

Manley, S.L., Wang, N.-Y., Walser, M.L., and Cicerone, R.J., 2006. Coastal salt marshes as global methyl halide sources from determinations of intrinsic production by marsh plants. Global Biogeochemical Cycles 20, GB3015, 13 p.

Mann, M.E., Zhang, Z., Rutherford, S., Bradley, R.S., Hughes, M.K., Shindell, D., Ammann, C., Faluvegi, G. and Ni, F., 2009. Global signatures of the Little Ice Age and Medieval climate anomaly and plausible dynamical origins, Science 326, 1256–1260.

Mayer, L.M., 1994. Relationships between mineral surfaces and organic carbon concentrations in soils and sediments. Chemical Geology 114, 347–363.

Mayer, L.M., Schick, L.L., Allison, M.A., Ruttenberg, K.C. and Bentley, S.J., 2007. Marine vs. terrigenous organic matter in Louisiana coastal sediments: The uses of bromine:organic carbon ratios. Marine Chemistry 107, 244–254.

1126 Mariscal, M.J., Orgaz, F. and Villalobos, F.J., 2000. Modelling and measurement of
1127 radiation interception by olive canopies. Agricultural and Forest Meteorology 100,183–197.
1128
1129 Marques, B., Lillebø A.I., Pereira, E. and Duarte, A.C., 2011. Mercury cycling and
1130 sequestration in salt marshes sediments: An ecosystem service provided by *Juncus*
1131 *maritimus* and *Scirpus maritimus*. Environmental Pollution 159, 1869–1876.
1132
1133 Martin-Puertas, C., Matthes, K., Brauer, A., Muscheler, R., Hansen, F., Petrick, C., Aldahan,
1134 A., Possnert, G. and van Geel, B., 2012. Regional atmospheric circulation shifts induced by
1135 a grand solar minimum. Nature Geoscience 5, 397–401.
1136
1137 Martínez-Cortizas, A., Vázquez, C.F., Kaal, J., Biester, H., Casais, M.C., Rodríguez, T.T.
1138 and Lado, L.R., 2016. Bromine accumulation in acidic black colluvial soils. Geochimica et
1139 Cosmochimica Acta 174, 143–155.
1140
1141 Martínez-Cortizas, A., Biester, H., Mighall, T. and Bindler, R., 2007. Climate-driven
1142 enrichment of pollutants in peatlands. Biogeosciences 4, 905–911.
1143
1144 Martins, F., Leitão, P., Silva, A. and Neves, R., 2001. 3D modelling in the Sado estuary
1145 using a new generic vertical discretization approach. Oceanologica Acta 24, 1–12.
1146
1147 Masarik, J. and Beer, J., 1999. Simulation of particle fluxes and cosmogenic nuclide
1148 production in the Earth's atmosphere. Journal of Geophysical Research 104, 12099–12111.
1149
1150 Meentemeyer, V., 1978. Macroclimate and lignin control of litter decomposition rates.
1151 Ecology 59, 465–472.

Millero, F.J., 2013. Chemical Oceanography, CRC Press, 4th edition, Boca Raton, 571 p.

Mineke, W. and Bakker, J.P., 2002. Soil seed bank and driftline composition along a successional gradient on a temperate salt marsh. Applied Vegetation Science 5, 55–62.

Moreira, M.E.S.A., 1992. Recent saltmarsh changes and sedimentation rates in the Sado estuary, Portugal. Journal of Coastal Research 8, 631–640.

Moreno, A., Pérez, A., Frigola, J., Nieto-Moreno, V., Rodrigo-Gámiz, M., González-Sampériz,
P., Morellón, M., Martín-Puertas, C., Corella, J.P., Belmonte, Á., Sancho, C., Cacho, I., Herrera, G., Canals, M., Jiménez-Espejo, F., Martínez-Ruiz, F., Vegas, T. and Valero Garcés,
B.L., 2012. The Medieval Climate Anomaly in the Iberian Peninsula reconstructed from marine and lake records. Quaternary Science Reviews 43, 16–32.

Moreno, J., Fatela, F., M.A. Gonçalves, M.A., Leorri, E., Gómez-Navarro, J.J., Brázdil, R., Ferreira, M.J., Moreno, F. and R. Trigo (submitted). A bi-proxy paleoclimatic reconstruction for the Entre-Douro-e-Minho region, northwest Portugal, from 1626 to 1820 – A search for evidence of solar forcing.

Moreno, J., Fatela, F., Leorri, E., Araújo, M.F., Moreno, F., De la Rosa, J.M., Freitas, M.C., Valente, T. and Corbett, R., 2015. Bromine enrichment in marsh sediments as a marker of environmental changes driven by Grand Solar Minima and Anthropogenic activity (Caminha, NW of Portugal). Science of the Total Environment 506–507, 554–566.

Moreno, J., Fatela, F., Leorri, E., De la Rosa, J., Pereira, I., Araújo, M.F., Freitas, M.C., Corbett, R. and Medeiros, A., 2014. Marsh benthic foraminifera response to estuarine hydrological balance driven by climate variability over the last 2000 years (Minho estuary, NW Portugal). Quaternary Research 82, 318–330.

Moreno, J., Fatela, F., Andrade, C., Cascalho, J., Moreno, F. and Drago, T., 2005. Living foraminiferal assemblages from the Minho and Coura estuaries (Northern Portugal): a stressful environment. Thalassas 21, 17–28.

Morrisey, E.M., Gillespie, J.L., Morina, J.C. and Franklin, R.B., 2014. Salinity affects microbial activity and soil organic matter content in tidal wetlands. Global Change Biology 20, 1351–1362.

Neubauer, S.C., Franklin, R.B. and Berrier, D.J., 2013. Saltwater intrusion into tidal freshwater marshes alters the biogeochemical processing of organic carbon Biogeosciences Discussions 10, 10685–10720.

Neukom, R. Gergis, J. 3, Karoly, D.J., Wanner, H., Curran, M., Elbert, J., González-Rouco, F., Linsley, B.K, Moy, A.D., Mundo, I.,10, Raible, C.C.,1,11, Steig, E.J., van Ommen, T., Vance, T. Villalba, R., Zinke, J. and Frank, D., 2014. Inter-hemispheric temperature variability over the past millennium. Nature Climate Change 4, 362–367.

Neuparth, T., Correia, A.D., Costa, F.O., Lima, G. and Costa, M.H., 2005. Multi-level assessment of chronic toxicity of estuarine sediments with the amphipod *Gammarus locusta*: I. Biochemical endpoints. Marine Environmental Research 60, 69–91.

Nittrouer, C.A., Sternberg, R.W., Carpenter, R. and Bennett, J.T., 1979. The use of ^{210}Pb geochronology as a sedimentological tool: application to the Washington Continental Shelf. Marine Geology 31, 297–316.

Obrist, D., Tas, E., Peleg, M., Matveev, V., Faïn, X., Asaf, D. and Luria, M., 2011. Bromine-induced oxidation of mercury in the mid-latitude atmosphere. Nature Geoscience 4, 22–26.

Panno, S.V., Hackley, K.C., Hwang, H.H., Greenberg, S.E., Krapac, I.G., Landsberger, S. and O'Kelly, D.J., 2006. Characterization and identification of Na-Cl sources in ground water. Ground Water 44, 176–187.

Parnell, A., Haslett, J., Allen, J., Buck, C. and Huntley, B., 2008. A flexible approach to assessing synchronicity of past events using Bayesian reconstructions of sedimentation history. Quaternary Science Reviews 27, 1872–1885.

Paula, J., Silva, I.C., Francisco, S.M. and Flores, A.V., 2006. The use of artificial benthic collectors for assessment of spatial patterns of settlement of megalopae of *Carcinus maenas* (L.) (Brachyura: Portunidae) in the lower Mira Estuary, Portugal. Hydrobiologia 557, 69–77.

Persicke, U., Gerlach, A. and Heiber, W., 1999. Zur botanischen Zusammensetzung von Treibsel der niedersachsischen Deichvorlander und Deichabsnitte. Drosera 1, 23–34.

Poffenbarger, H.J., Needelman, B.A. and Megonigal, J.P., 2011. Salinity influence on methane emissions from tidal marshes. Wetlands 31, 831–842.

Raimund, S., Quack, B., Bozec, Y., Vernet, M., Rossi, V., Garçon, V., Morel, Y. and Morin P., 2011. Sources of short-lived bromocarbons in the Iberian upwelling system. Biogeosciences 8, 1551–1564.

Reis, P.A., Guilhermino. L., Antunes, C., and Sousa, R., 2014. Assessment of the ecological quality of the Minho estuary (Northwest Iberian Peninsula) based on metal concentrations in sediments and in *Corbicula fluminea*. Limnetica 33, 161–174.

Rhew, R.C., Whelan, M.E. and Min, D.-H., 2014. Large methyl halide emissions from south Texas saltmarshes. Biogeosciences 11, 6427–6434.

Rhew, R.C. and Mazéas, O., 2010. Gross production exceeds gross consumption of methyl halides in northern California salt marshes. Geophysical Research Letters 37, L18813, 5 p.

Rhew, R.C., Miller, B.R., Bill, M., Goldstein, A.H. and Weiss, R.F., 2002. Environmental and biological controls on methyl halide emissions from southern California coastal salt marshes. Biogeochemistry 60, 141–161.

Rhew, R.C., Miller, B.R. and Weiss, R.F., 2000. Natural methyl bromide and methyl chloride emissions from coastal salt marshes. Nature 403, 292–295.

Roberts, T.J., Martin, R.S. and Jourdain, L., 2014. Reactive bromine chemistry in Mount Etna's volcanic plume: the influence of total Br, high-temperature processing, aerosol loading and plume–air mixing. Atmospheric Chemistry and Physics 14, 11201–11219.

1256 Saito, T. and Yokouchi, Y., 2006. Diurnal variation in methyl halide emission rates from
1257 tropical ferns. Atmospheric Environment 40, 2806–2811.
1258
1259 Shaw, S.D., Blum, A., Weber, R., Kannan, K., Rich, D., Lucas, D., Koshland, C.P., Dobraca,
1260 D., Hanson, S. and Birnbaum, L.S., 2010. Halogenated flame retardants: do the fire safety
1261 benefits justify the risks? Reviews on Environmental Health 25, 261–305.
1262
1263 Smith, J.N., 2001. Why should we believe ^{210}Pb sediment geochronologies? Journal of
1264 Environmental Radioactivity 55, 121–123.
1265
1266 Soon, W., Velasco Herrera, V.M., Selvaraj, K., Traversi, R., Usoskin, I., Chen, C.-T.A., Lou,
1267 J.-Y., Kao, S.-J., Carter, R.M., Pipin, V., Severi, M. and Becagli, S., 2014. A review of
1268 Holocene solar-linked climatic variation on centennial to millennial timescales: physical
1269 processes, interpretative frameworks and a new multiple cross-wavelet transform algorithm.
1270 Earth Science Reviews 134, 1–15.
1271
1272 Spohn, M., Babka, B. and Giani, L., 2013. Changes in soil organic matter quality during sea-
1273 influenced marsh soil development at the North Sea coast. Catena 107, 110–117.
1274
1275 Spohn, M. and Giani, L., 2012. Carbohydrates, carbon and nitrogen in soils of a marine and
1276 a brackish marsh as influenced by inundation frequency. Estuarine, Coastal and Shelf
1277 Science 107, 89–96.
1278
1279 Steinhilber, F., Abreu, J.A., Beer, J., Brunner, I., Christl, M., Fischer, H., Heikkilä, U., Kubik,
1280 P.W., Mann, M., McCracken, K.G., Miller, H., Miyahara, H., Oerter, H. and Wilhelms, F.,

1281 2012. 9,400 years of cosmic radiation and solar activity from ice cores and tree rings.
1282 Proceedings of the National Academy of Sciences 109, 5967–5971.
1283
1284 Usoskin, I.G. and Kovaltsov, G.A., 2008. Cosmic rays and climate of Earth: Possible
1285 connection, Comptes Rendus Geoscience 340, 441–450.
1286
1287 Vale, L.M. and Dias, J.M., 2011. The effect of tidal regime and river flow on the
1288 hydrodynamics and salinity structure of the Lima Estuary: Use of a numerical model to
1289 assist on estuary classification, SI 64 (Proceedings of the 11th International Coastal
1290 Symposium), Szczecin, Poland, pp. 1604–1608.
1291
1292 Taborda, R., Dias, J.M.A., 1991. Análise da sobre-elevação do nível do mar de origem
1293 meteorológica durante os temporais de 1978 e 1981. Geonovas, SI 1, 89–97.
1294
1295 Thiéblemont, R., Matthes, K., Omrani, N.-E., Kodera, K. and Hansen, F., 2015. Solar forcing
1296 synchronizes decadal North Atlantic climate variability. Nature Communications 6:8268. 8 p.
1297
1298 Trigo, R.M., Vaquero, J.M., Alcoforado, M.J., Barriendos, M., Taborda, J., García-Herrera R.
1299 and Luterbacher, J., 2009. Iberia in 1816, the year without a summer. International Journal
1300 of Climatology 29, 99–115.
1301
1302 Van de Broek, M., Temmerman, S., Merckx, R. and Govers, G., 2016. The importance of an
1303 estuarine salinity gradient on soil organic carbon stocks of tidal marshes. Biogeosciences
1304 Discussions, doi:10.5194/bg-2016-285.
1305

Varner, R.K., Crill, P.M. and Talbot, R.W., 1999. Wetlands: A potentially significant source of atmospheric methyl bromide and methyl chloride, Geophysical Research Letters 26, 2433– 2435.

Vinogradov, A.P., 1959. The Geochemistry of Rare and Dispersed Elements in Soils. Second edition, Consultants Bureau, New York, 209 p.

Weinberg, I., Bahlmann, E., Eckhardt, T., Michaelis, W. and Seifert, R., 2015. A halocarbon survey from a seagrass dominated subtropical lagoon, Ria Formosa (Portugal): flux pattern and isotopic composition. Biogeosciences 12, 1697–1711.

Weinberg, I., Bahlmann, E., Michaelis, W. and Seifert, R., 2013. Determination of fluxes and isotopic composition of halocarbons from seagrass meadows using a dynamic flux chamber. Atmospheric Environment 73, 34–40.

Wishkerman, A., Gebhardt, S., McRoberts, C.W., Hamilton, J.T.G., Williams, J. and Keppler, F., 2008. Abiotic methyl bromide formation from vegetation and its strong dependence on temperature. Environmental Science & Technology 42, 6837–6842.

Wuosmaa, A. M. and Hager, L. P., 1990. Methyl chloride transferase: a carbocation route for biosynthesis of halometabolites, Science 249, 160–162.

Yvon-Lewis, S.A., Saltzman, E.S. and Montzka, S.A., 2009. Recent trends in atmospheric methyl bromide: analysis of post-Montreal Protocol variability. Atmospheric Chemistry and Physics 9, 5963–5974.

Ziegler, M., Jilbert, T., de Lange, G.J., Lourens L.J. and Reichart, G.-J., 2008. Bromine counts from XRF scanning as an estimate of the marine organic carbon content of sediment cores. Geochemistry Geophysics Geosystems 9, Q05009, 6 p.

http://www.icnf.pt/portal/ap/r-nat/rnet/geo

http://www.noaa.gov/

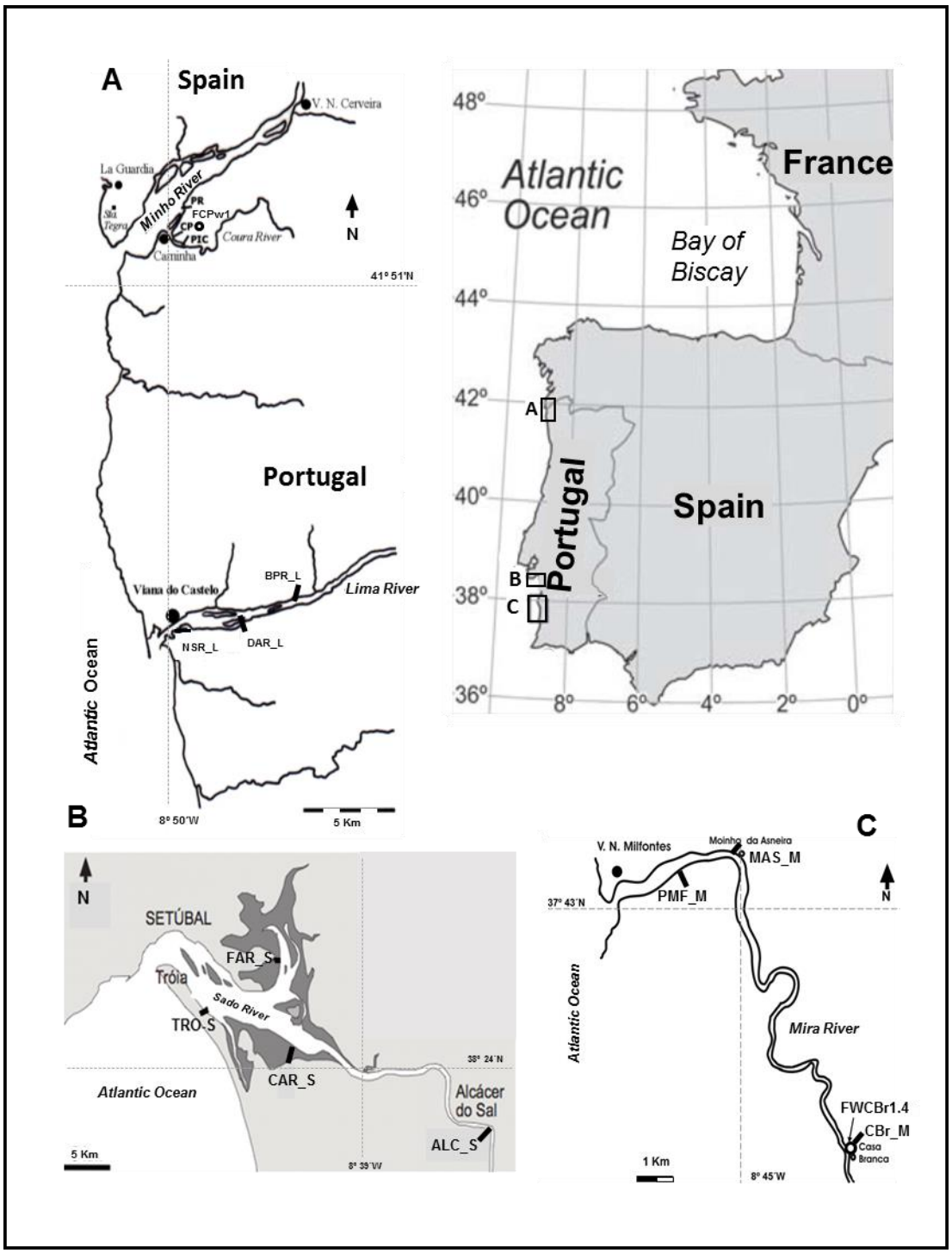

Figure 1. A. Study areas general location; B. Minho and Lima estuaries (NW coast); C. Sado estuary (SW coast); D. Mira estuary (SW coast). The location of the complete sampling set is also signalled. This includes thirteen surface sampling transects across the four tidal salt marshes (where both interstitial waters and sediments have been collected), and the two sediment cores obtained in the high marsh zones of the Caminha (FCPw1; Minho estuary; 1.55 m above mean sea level; 41°52′37.0″ N and 8°49′28.0″ W) and Casa Branca (FWCBr1.4; Mira estuary; 1.74 m above mean sea level; 37°40′03.7″ N and 8°43′12.7″ W) salt marshes.

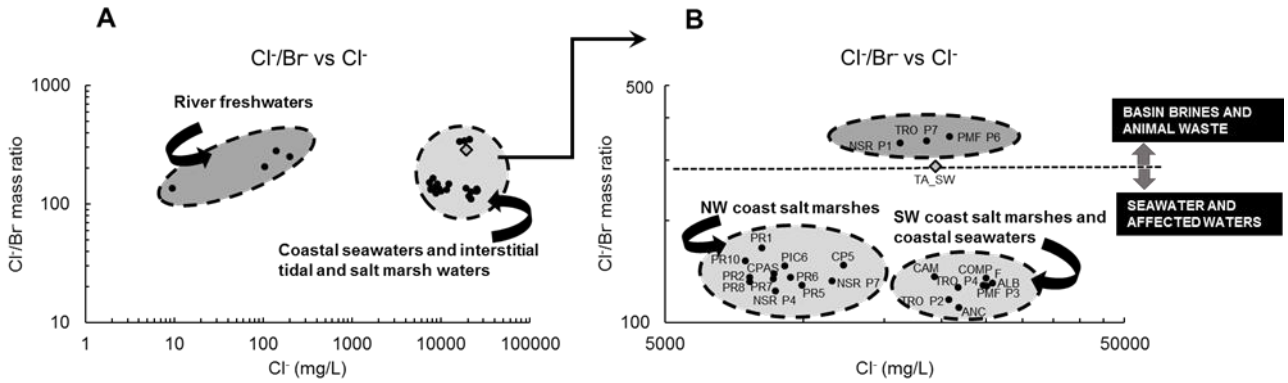

Figure 2. Cl^-/Br^- mass ratios vs. Cl^- concentrations of (surface and interstitial) water samples and potential sources (zones and theoretical limits from Panno et al., 2006). **A.** Clusters of freshwater (riverine), marine, and impacted water samples are indicated (i.e., tidal and salt marsh interstitial waters). **B.** Clusters of interstitial waters from NW and SW coastal salt marshes. Marine water samples are in the same group as the SW coast salt marshes interstitial water. A group of three anomalous samples (TRO_P7, NSR_P1 and PMF_P6) is also identified. The diamond represents a typical marine sample**.**

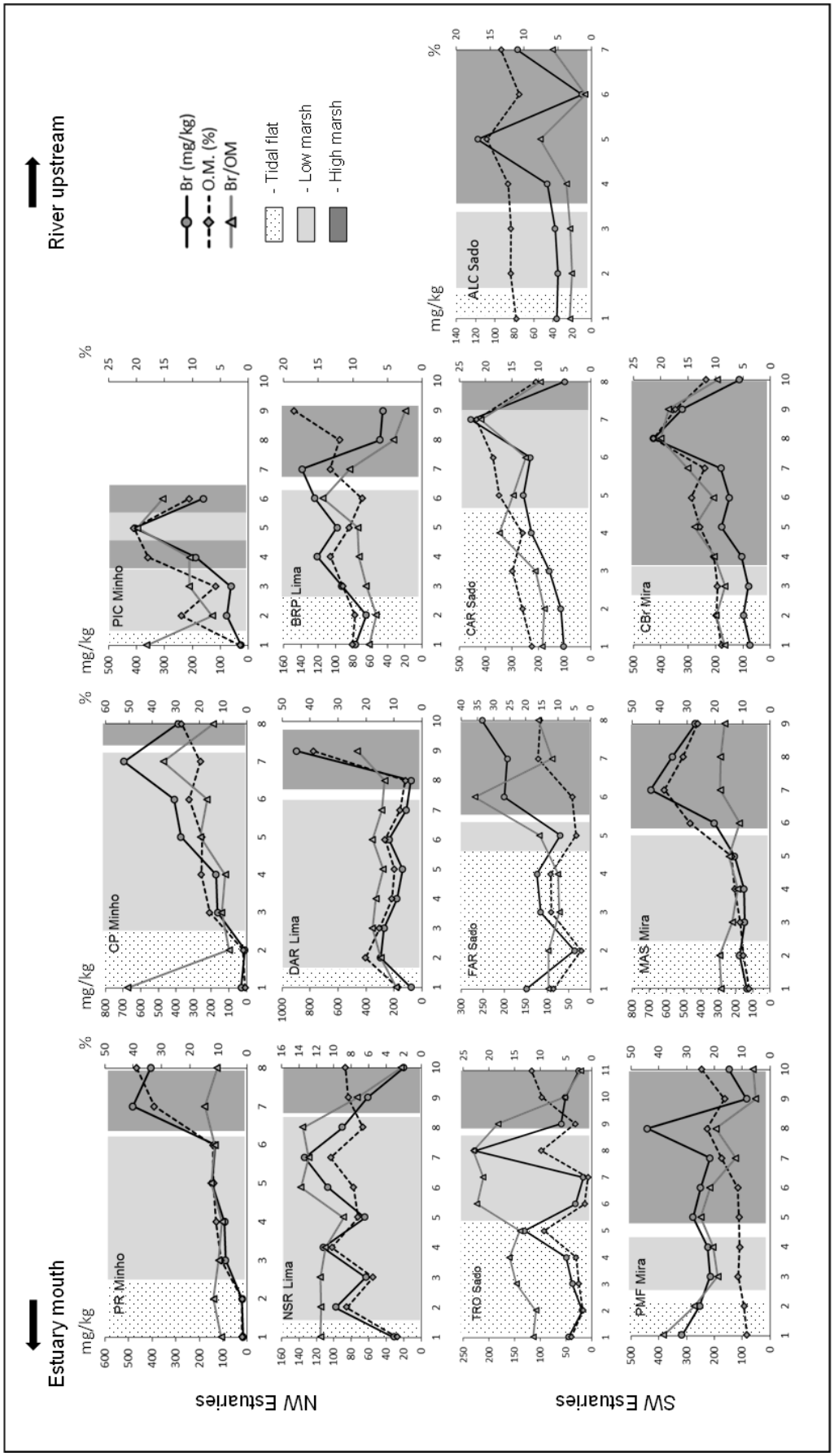

Figure 3. Bromine and organic matter contents (OM) of superficial tidal salt marsh sediment transects from Minho, Lima, Sado and Mira estuaries.

1361

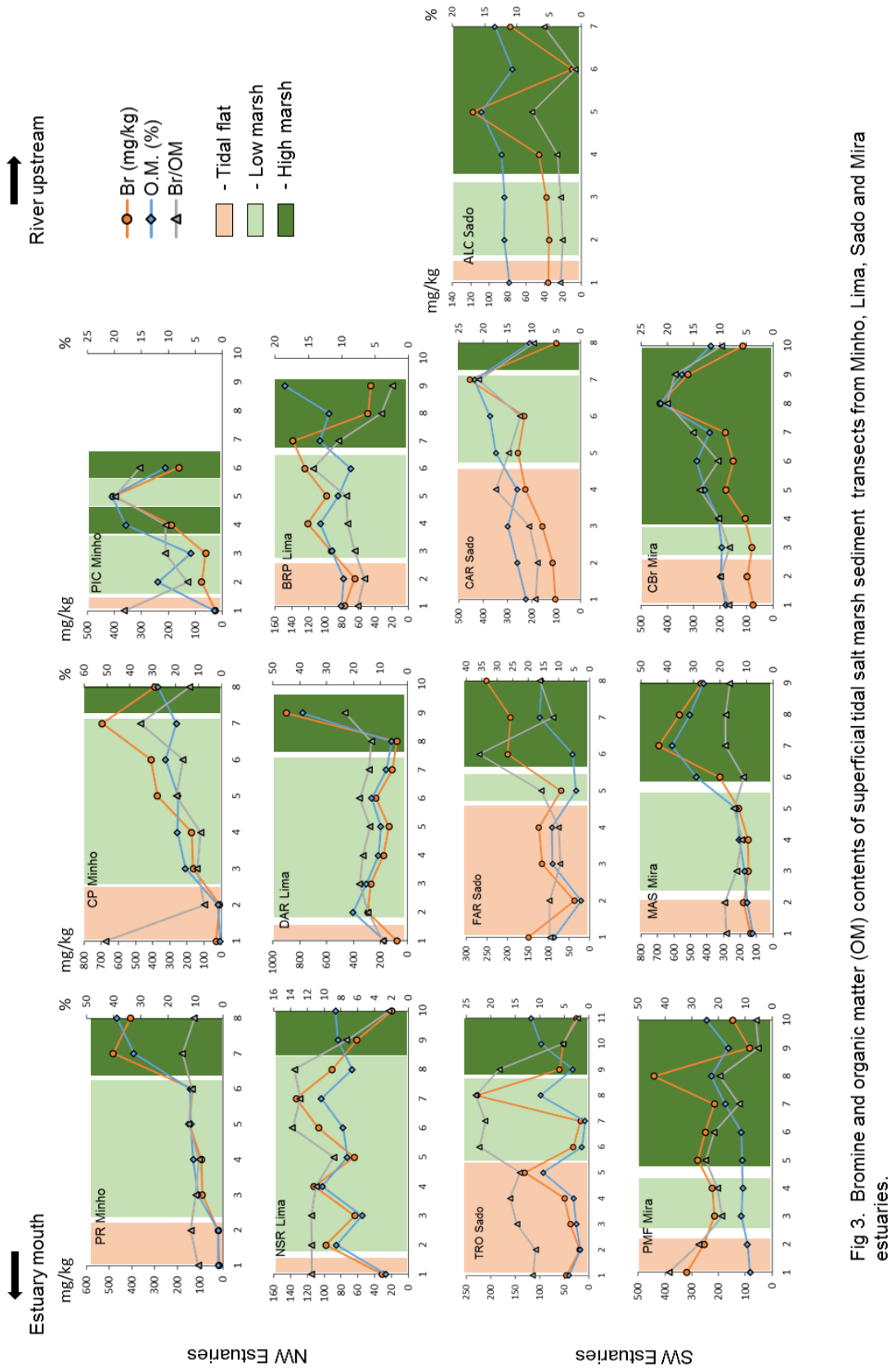

Fig 3. Bromine and organic matter (OM) contents of superficial tidal salt marsh sediment transects from Minho, Lima, Sado and Mira estuaries.

1362

1363

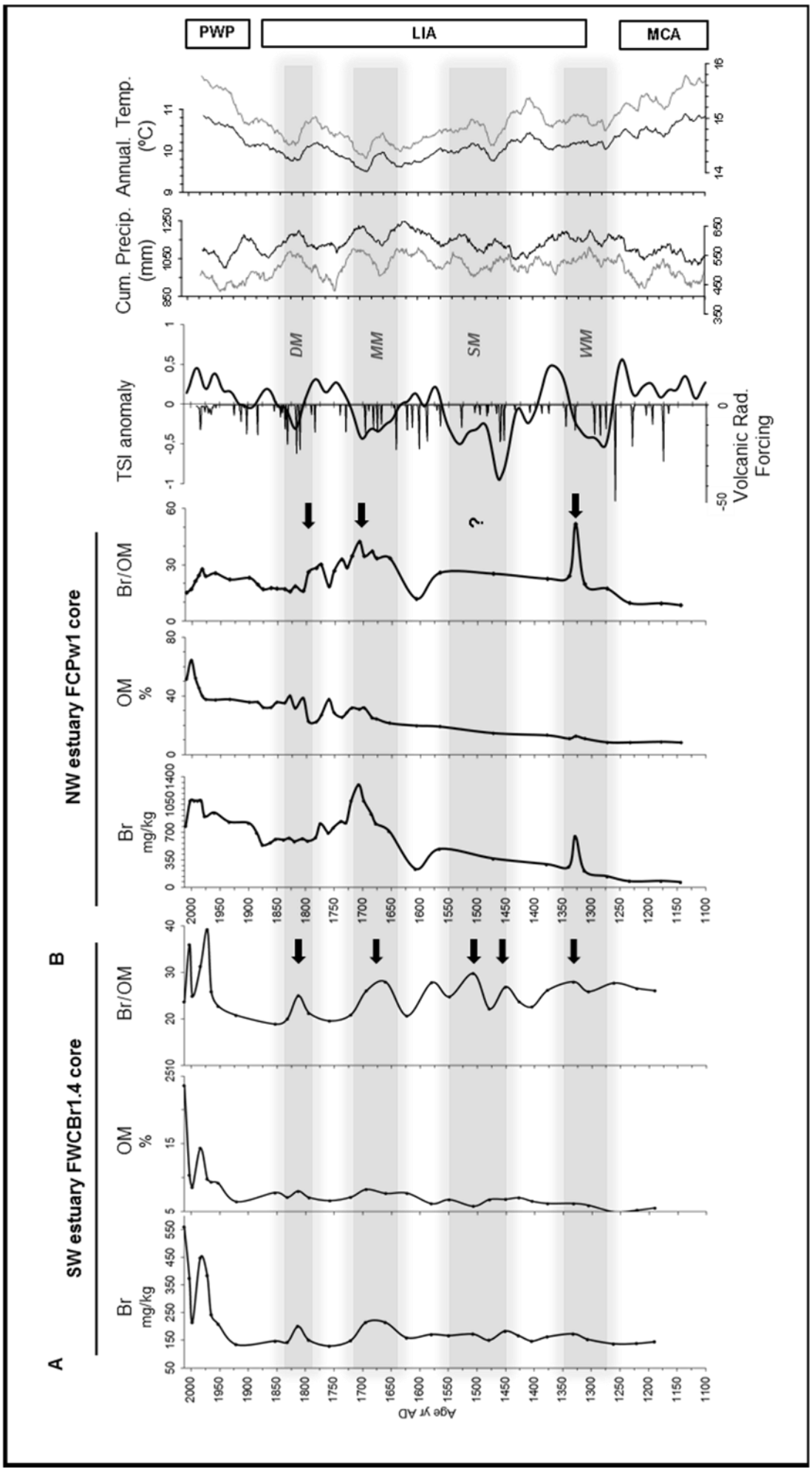

Figure 4. FCPw1 and FWCBr1.4 cores geochemical data: Br (mg/kg), OM (%) and Br/OM ratios. Other data represented are: TSI anomaly using a 21-year running average reconstruction (Steinhilber et al., 2012); volcanic radiative forcing (black bars) after Crowley (2000); cumulative precipitation and annual temperature (31-year running averages) for NW coast (black lines and top axis) and SW coast (grey lines and bottom axis) of Portugal (Gómez-Navarro et al., 2011). DM – Dalton Minimum; MM – Maunder Minimum; SM – Spörer Minimum; WM – Wolf Minimum.

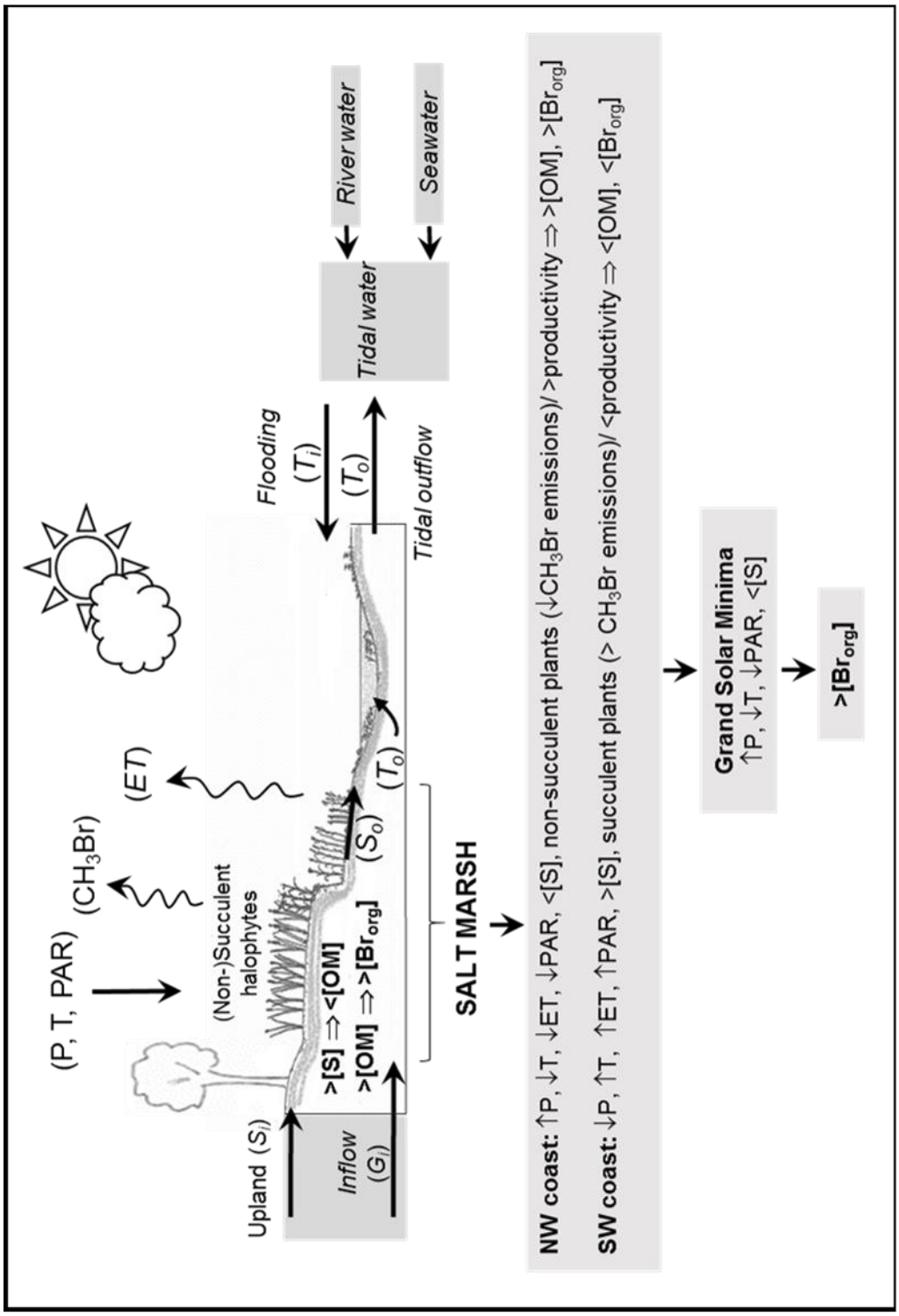

Figure 5. Conceptual model for the Br cycling in the W Portuguese coast salt marshes, including the most important elements influencing the Br pool in soils/sediments. (P– Precipitation; T– Temperature; PAR– Photosynthetically Active Radiation; ET– Evapotranspiration; S_i– Surface water inflow; S_o– Surface water outflow; G_i– Ground water inflow; T_i– Tidal water outflow; T_o– Tidal water outflow; [S]– Salinity; [OM]– Soil/Sediment Organic Matter content; $[Br_{org}]$– Soil/Sediment Organic Bromine content).

Table 1. Bromide concentrations in surface water (river freshwater, estuarine and coastal seawater) samples and in marsh interstitial water samples (Minho, Lima, Sado and Mira tidal salt marshes).

Surface and interstitial waters	NW coast				SW coast			
	Minho		Lima		Sado		Mira	
Zone	Br^- (mg/L)	Salinity (‰)	Br^- (mg/L)	Salinity (‰)	Br^- (mg/L)	Salinity (‰)	Br^- (mg/L)	Salinity (‰)
River	<d.l.	0.0	0.07	0.0	0.8	0.3	0.5	0.2
Estuary mouth	141	32.5	—	—	—	—	—	—
Coastal seawater	197	35.2	197	35.2	185	35.7	197	35.4
Tidal flat	52 (48-55)*	9.5 (2-17)*	48	24.6	177	31.8	—	—
Low marsh	71 (64-83)*	14.5 (10-18)*	70	14.4	171	31.4	195	37.0
High marsh	56 (49-62)*	12.6 (11-15)*	87	13.5	54	26.6	59	30.6
Marsh transect references	PR; CP; PIC		NSR-L		TRO-S		PMF-M	
Distance to river mouth (km)	3.8 - 4.8		2.0		14.0		2.0	

*Average from three transects and range

d.l. detection limit (0.01 mg/L Br^-)

Table 2. Bromine content and OM contents in the surface sediment cross shore transects from the Minho, Lima, Sado and Mira intertidal domains (tidal flat, low marsh and high marsh).

Surface sediment samples / Estuaries	NW coast				SW coast			
	Minho		Lima		Sado		Mira	
Zone	Br (mg/kg)	OM (%)	Br (mg/kg)	OM (%)	Br (mg/kg)	OM (%)	Br (mg/kg)	OM (%)
Tidal Flat	21 (11-30)*	1.4 (0.6-1.7)*	71 (31-79)*	8.6 (2.7-10.1)*	83 (19-226)**	11.5 (1.7-15.0)**	158 (75-318)*	8.8 (7.7-9.9)*
Low Marsh	133 (62-695)*	15.0 (5.9-24.4)*	110 (64-296)*	11.0 (5.5-20.2)*	53 (17-456)**	8.2 (0.8-21.8)**	152 (80-224)*	11.2 (9.7-12.8)*
High Marsh	389 (162-482)*	27.7 (10.6-38.8)*	49 (45-900)*	13.3 (5.9-38.9)*	81 (10-252)**	11.7 (3.3-16.3)**	233 (85-693)*	16.9 (11.2-38.3)*
Marsh transect/cores surface references	PR; CP; PIC		NSR_L; DAR_L; BPR_L		TRO_S; CAR_S; FAR_S; ALC_S		PMF_M; MAS_M; CBr_M	
Distance to river mouth (km)	3.8 - 4.8		2; 5; 8.5		14; 19; 24; 43.5		2; 3.5; 13	
Correlation coeficient Br vs.OM (p < 0.001)	0.86 (N= 21)		0.89 (N= 28)		0.67 (N= 34)		0.79 (N= 29)	

*Average (median) from three transects and range

**Average (median) from four transects and range

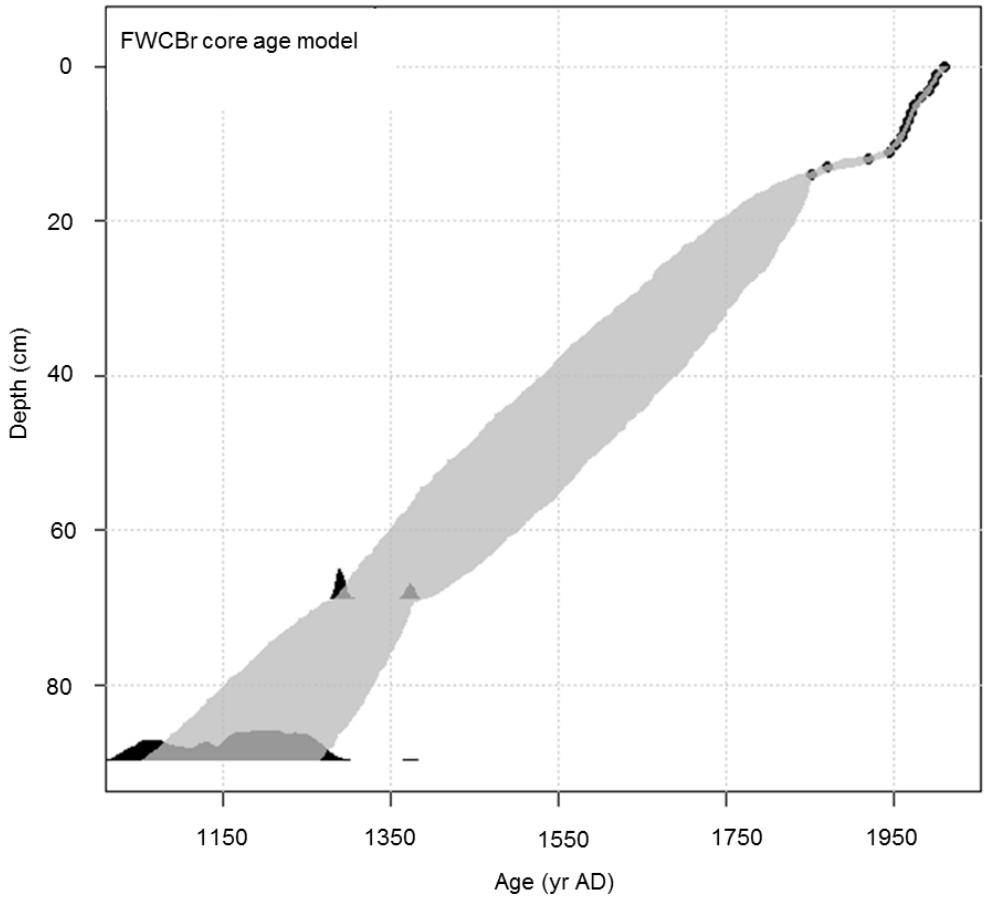

Depth (cm)	^{137}Cs	2-sigma	^{210}Pb	2-sigma	^{214}Pb	2-sigma	^{210}Pb $_{excess}$
0.5	5.56	2.27	152.5	30.6	37.5	6.76	115
1.5	5.44	1.6	84.52	20.11	40.02	3.78	44.5
2.5	6.95	1.63	72.48	20.36	38.38	3.9	34.1
3.5	8.78	2.13	98.24	21.85	37.22	5.58	61.02
4.5	10.64	2.18	70.55	21.47	34.65	5.25	35.9
5.5	13.23	2.23	53.13	21.05	32.45	4.79	20.68
6.5	19.19	2.32	48.51	25.88	34.29	3.97	14.22
7.5	23.69	2.73	46.97	17.43	36.53	6.44	10.44
8.5	14.41	2.04	54.26	18.92	42.94	5.77	11.32
9.5	6.74	1.81	58.57	20.37	41.42	4.24	17.15
10.5	6.4	1.72	52.57	18.23	40.33	4.8	12.24
11.5	5.45	1.65	65.43	19.23	41.41	3.99	24.02
12.5	2.92		65.13	22.17	47.18	4.21	17.95
13.5	2.37		53.57	21.12	51.31	5.19	2.26
14.5	2.58		56.08	21.57	52.17	5.83	3.91
15.5	2.5		41.48	19.35	43.05	4.29	-1.57

Pb and Cs isotopes contents (Bq kg−1)

Core/Sample	Depth (cm)	δ^{13}C ‰	Conventional radiocarbon age	Δ^{14}C ‰	Calibrated years AD (2 Sigma range)
FW CBr 2.0 CM 70	69-70	-25.0	720 +/- 30 BP	-85.7±3.4	1260 to 1295
FW CBr 2.0 CM 91	90-91	-25.6	920 +/- 30 BP	-108.2±3.3	1025 to 1190

Appendix A. Age model for the core FWCBr and estimated 2 σ errors, based on two AMS ^{14}C dates, performed on total organic sediment, and ^{210}Pb and ^{137}Cs chronology. The data interpolation was obtained with Bchron 4.1 software.

Appendix B. Geochemical data from the sediment core FWCBr (Casa Branca salt marsh; Mira estuary).

Depth (cm)	Br (ppm)	OM (%)	Br/OM	Age (AD years)
0-1	560	23.6	23.7	2012
1-2	374	10.4	36.0	2003
2-3	214	8.6	24.9	1998
4-5	448	14.3	31.2	1984
6-7	385	9.8	39.3	1972
8-9	242	9.4	25.8	1965
10-11	209	9.2	22.7	1953
12-13	134	6.5	20.7	1921
14-15	147	7.8	18.8	1853
16-17	142	7.1	20.0	1832
18-19	200	8.0	24.9	1813
20-21	150	7.1	21.2	1794
24-25	129	6.6	19.5	1758
28-29	149	7.1	20.9	1721
31-32	215	8.3	26.0	1694
35-36	214	7.7	27.9	1660
39-40	159	7.7	20.6	1623
43-44	171	6.2	27.8	1580
47-48	167	6.7	24.8	1549
52-53	172	5.8	29.7	1507
55-56	150	6.8	22.1	1479
58-59	183	6.8	26.9	1451
61-62	166	7.0	23.6	1427
64-65	147	6.5	22.6	1404
68-69	162	6.2	26.2	1377
72-73	173	6.2	28.0	1332
75-76	153	5.9	25.9	1306
80-81	137	4.9	27.7	1261
85-86	138	5.2	26.5	1221
89-90	144	5.5	26.0	1190